Chapter 4

Impact of Sulfur and Phosphorus Lubrication Additives and their Thermal Decomposition Products on 55Al-43.4Zn-1.6Si Metallic Coating Quality

Preface

Thermogravimetric Analysis (TGA) and Pressure Differential Scanning Calorimetry (PDSC) techniques are used to examine the thermo-oxidative and -reductive decomposition processes undergone by four sulfur-based (4.1) and two phosphorus-based (4.2) extreme pressure lubrication additives. Ramped heating conditions are used to mimic the continuous annealing process, whereby rolling oil is removed from the surface of cold rolled steel strip. Relationships between sulfur/phosphorus functionalities present in the additive structures and the chemical nature of thermally stable residue present at high temperatures (~ 500 ^{o}C, the average maximum temperature employed during continuous annealing) are assessed by mass spectrometric (sulfur additives) and infrared (sulfur and phosphorus additives) techniques. The impact of additive chemical structure and concentration on the oxidative stability (sulfur additives) and residue-forming tendencies (sulfur and phosphorus additives) of a commercial base ester are determined from the thermal analysis results and the effect of persistent decomposition deposits on 55Al-43.4Zn-1.6Si coating quality is ascertained by performing experimental hot dipping simulations. The results show that significant amounts of soap-like residues are formed by the decomposition of sulfurised triglycerides (‘inactive’ sulfur). These residues have a greater detrimental impact upon 55Al-43.4Zn-1.6Si metallic coating quality than the sulfide/sulfur oxide residues formed by sulfurised hydrocarbons (‘active’ sulfur). Sulfurised hydrocarbons can be incorporated into a commercial base ester at much higher concentrations than sulfurised triglycerides without increasing the amount or thermal stability of residue formed by ester decomposition and ultimately, the level of uncoated defects. Similarly, although the

phosphorus-based lubrication additives change the chemical composition and increase the amount of residue formed by commercial base ester decomposition, they have minimal effect on hot dip metallic coating quality even at high (2.5 % w/w) phosphorus concentration.

4.1 Links between Sulfurised Lubrication Additive Chemical Structure, the Formation of Thermally-Stable Decomposition Deposits and 55Al-43.4Zn-1.6Si Coating Quality

4.1.1 Introduction

During the steel cold rolling process, high tension and compression forces are applied to the strip in order to achieve a reduction in thickness. The incorporation of extreme-pressure (EP) lubrication additives into cold rolling oil formulations arises from the need to lower the frictional forces between the roll surface and the steel strip and reduce the amount of work that must be done to accomplish strip reduction.[1] Organo-sulfur compounds are one of the most widely employed groups of cold rolling EP additives[2-5] and typically constitute ~ 1 % w/w of a cold rolling oil formulation.[3] Whilst the thermal decomposition of sulfur additives is critical to their cold rolling lubrication performance,[1, 3, 4, 6] it has been linked to the formation of sludge-like deposits under oxidising conditions.[7, 8] Given the importance of surface cleanliness to the integrity of coatings placed onto the surface of cold rolled steel strip after the cold rolling and furnace cleaning processes,[9-11] the thermo-oxidative and -reductive decomposition properties of sulfur additives used in cold rolling oil formulations are of critical importance to final product quality.

Sulfur is typically incorporated into sulfurised EP additives in the form of n-sulfide bridges between adjacent hydrocarbon chains (n = 1-5),[2-5] although other sulfur functionalities such as thiophenes may also be present.[12] Scheme 1.21 in Chapter 1 shows the representative chemical structures of two of the most common classes of sulfur EP additives, sulfurised hydrocarbons and sulfurised triglycerides. The primary difference between sulfurised hydrocarbons and sulfurised triglycerides lies in the surface activity of their sulfur groups. The ‘active’ n-sulfide bridges in sulfurised

hydrocarbons readily decompose to form alkylthiyl radical species ($RS^{\bullet}$) which bind directly to metal surfaces.[4] In contrast, the ester carboxyl groups present in sulfurised triglycerides initially adhere to metal surfaces and the application of high temperatures and/or pressures is required to effect interactions between the 'inactive' sulfur chains and the surface.[13] Despite these differences, the decomposition of both types of additives results in the formation of a protective film that lowers the coefficient of friction.[1, 14-16] Although the precise composition of this film depends upon numerous parameters including temperature,[1, 6, 17] applied load/pressure[3, 4] and the additive chemical structure,[1] it generally contains a mixture of metal oxides, sulfides and sulfates.[1, 3, 4, 6, 17]

Whilst the impact of sulfurised additive decomposition deposits on oil lubrication performance has been studied in detail,[1, 3, 4, 6] little has been done to establish whether a relationship exists between the presence and chemical nature of such deposits and the quality of subsequent coatings placed onto the cold rolled steel surface. Furthermore, knowledge gaps exist concerning the effect of sulfur additives on the residue-forming tendencies of cold rolling oils; although the beneficial effect of sulfur additives in reducing levels of carbonaceous deposits formed by rolling oil decomposition under batch annealing (HNX, thermo-reductive) conditions is well-documented,[13] the behaviour of these additives under continuous annealing (natural gas combustion products, thermo-oxidative) conditions has not been studied.

Organo-sulfur compounds have been found to greatly increase the deposit-forming tendencies of fuels,[7, 8, 18] however the processes via which these deposits are formed together with their chemical structure and dependency on sulfur additive chemistry have not been investigated. In addition, although the thermal decomposition of a range of organo-sulfur compounds has been studied under inert conditions[19, 20] and under oxidising conditions through the use of wet chemical procedures,[5, 7, 8, 18] very little work has been done under a continuous heating regime or using instrumental thermal analysis techniques.[2, 12]

In this study, the thermo-oxidative and -reductive decomposition processes undergone by four sulfurised EP lubrication additives commonly employed in commercial cold rolling oil formulations, sulfurised vegetable oil (SVO), sulfurised lard oil (SLO),

dialkyl pentasulfide (DAPS) and di-tert-dodecyl trisulfide (TSP 20), are examined by TGA and PDSC. The chemical nature of residues present at different stages throughout the decomposition process is characterised by mid- and far-infrared Attenuated Total Reflectance Spectroscopy (ATR). The influence of sulfur additive chemical structure and concentration on the oxidative stability and residue-forming tendencies of a representative commercial cold rolling base ester are also assessed. Relationships between sulfur additive chemistry, concentration and residue levels and 55Al-43.4Zn-1.6Si hot dip metallic coating quality have been evaluated through the performance of simulated hot dipping trials with optical microscopy analysis of the resultant coated samples. Finally, Time-of-Flight Secondary Ion Mass Spectrometry (ToF-SIMS) analysis of surface residues present in uncoated areas on the hot dipped samples has provided further insight into the chemical nature of the contaminants responsible for poor steel surface wettability by the molten alloy.

4.1.2 Experimental

4.1.2.1 Sample Preparation

4.1.2.1.1 Materials

SLO, SVO, DAPS and TPS 20 were supplied by Quaker Chemical (Australasia) and were used as received. The chemical structures of SLO, SVO and DAPS are proprietary, however general structural representations are given in scheme 1.2.1 in Chapter 1 and the structure of TPS 20 is given by (A) when R = R' = $(CH_2)_{11}C(CH_3)_3$. All four sulfurised additives are mixtures containing a distribution of sulfide chain lengths. Table 4.1 summarises the total concentration of sulfur (% w/w) contained in each additive.

Table 4.1 Total concentration of sulfur in each of the sulfurised EP additives.

Additive	Sulfur Concentration (% w/w)
DAPS	40
TPS 20	20
SVO	10
SLO	10

The chemical characteristics of ester A, a typical commercial cold rolling oil base ester, are described in Chapter 3 (refer to section 3.2.2.1.1).

The properties of the other materials used are described in Chapter 2.2 as follows:

- cold rolled steel - table 2.3;
- 55Al-43.4Zn-1.6Si alloy - table 2.4;
- shellite and ethanol solvents - section 2.2.5;
- oxygen and HNX gases - section 2.2.6, and
- TGA and PDSC consumables - section 2.2.7.

4.1.2.1.2 Sulfurised Additive/Ester A Blends

Blends of each of the sulfurised additives in commercial base ester A at 0.1, 0.5, 1.0, 2.5, 5.0 and 8.0 % w/w sulfur concentration were prepared according to the method described in Chapter 2 (refer to section 2.3.1.2).

4.1.2.1.3 Sample Preparation for ATR

Additive samples for mid- and far-infrared ATR analysis were prepared according to the procedure described in Chapter 2 (refer to section 2.3.2). Additional thermo-oxidatively decomposed samples were prepared for DAPS and TPS 20 at temperatures of 175 ^{o}C, 205 ^{o}C, 215 ^{o}C and 230 ^{o}C due numerous chemical changes occurring over the range 150-250 ^{o}C.

4.1.2.1.4 Preparation of Hot Dip Simulation Samples

55Al-43.4Zn-1.6Si hot dip metal-coated samples were created using neat sulfurised additives and their blends in commercial base ester A according to the hot dip simulation procedure described in Chapter 2 (refer to section 2.3.3).

4.1.2.2 Characterisation Techniques

4.1.2.2.1 TGA

The thermo-oxidative decomposition profiles of the neat sulfurised additives and their ester A blends and the thermo-reductive decomposition profiles of the neat sulfurised

additives were analysed by TGA under oxygen and HNX respectively according to the conditions and procedure described in Chapter 2 (refer to section 2.4.1).

4.1.2.2.2 PDSC

PDSC analysis of the neat sulfurised additives and their ester A blends was performed according to the procedure described in Chapter 2 (refer to section 2.4.2).

4.1.2.2.3 ATR

The parameters used to collect mid- and far-infrared ATR spectra of the neat and thermo-oxidatively decomposed sulfurised additives are described in Chapter 2 (refer to section 2.4.3).

4.1.2.2.4 Hot Dip Simulation Samples

The 55Al-43.4Zn-1.6Si coating integrity was analysed by optical microscopy and the % uncoated defect area for each sample was calculated according to the method described in Chapter 2 (refer to section 2.4.4). ToF-SIMS was used to identify the surface chemistry within uncoated areas in three representative hot dip simulation samples as described in Chapter 2 (refer to section 2.4.4.2).

4.1.3 Results and Discussion

4.1.3.1 Thermo-Oxidative Decomposition Profile

4.1.3.1.1 TGA

The TGA results obtained for TPS 20 and SLO under oxygen are representative of those obtained for DAPS and SVO. Figure 4.1 presents the mass loss (TG) and first derivative of mass loss (DTG) curves obtained. A summary of the onset points (T_{onset}), peak and shoulder temperatures (T_{max}), relevant mass losses and % residue values at 500 ^{o}C (the average maximum temperature employed during the continuous annealing process) is given in table 4.2.

The thermo-oxidative decomposition processes undergone by SLO and TPS 20 are remarkably different. TPS 20, which contains 20 % w/w ‘active’ sulfur in the form of

trisulfide bridges between its hydrocarbon chains, displays a single mass loss event that occurs at an average onset temperature of 172 ^{o}C, a peak temperature of 213 ^{o}C and corresponds to 97.2 % mass loss. The DTG curve shape is analogous to that reported for methyl stearate in Chapter 3.1 and the thermo-oxidative decomposition process is essentially complete at 230 ^{o}C with only 2.1 % residue remaining at 500 ^{o}C.

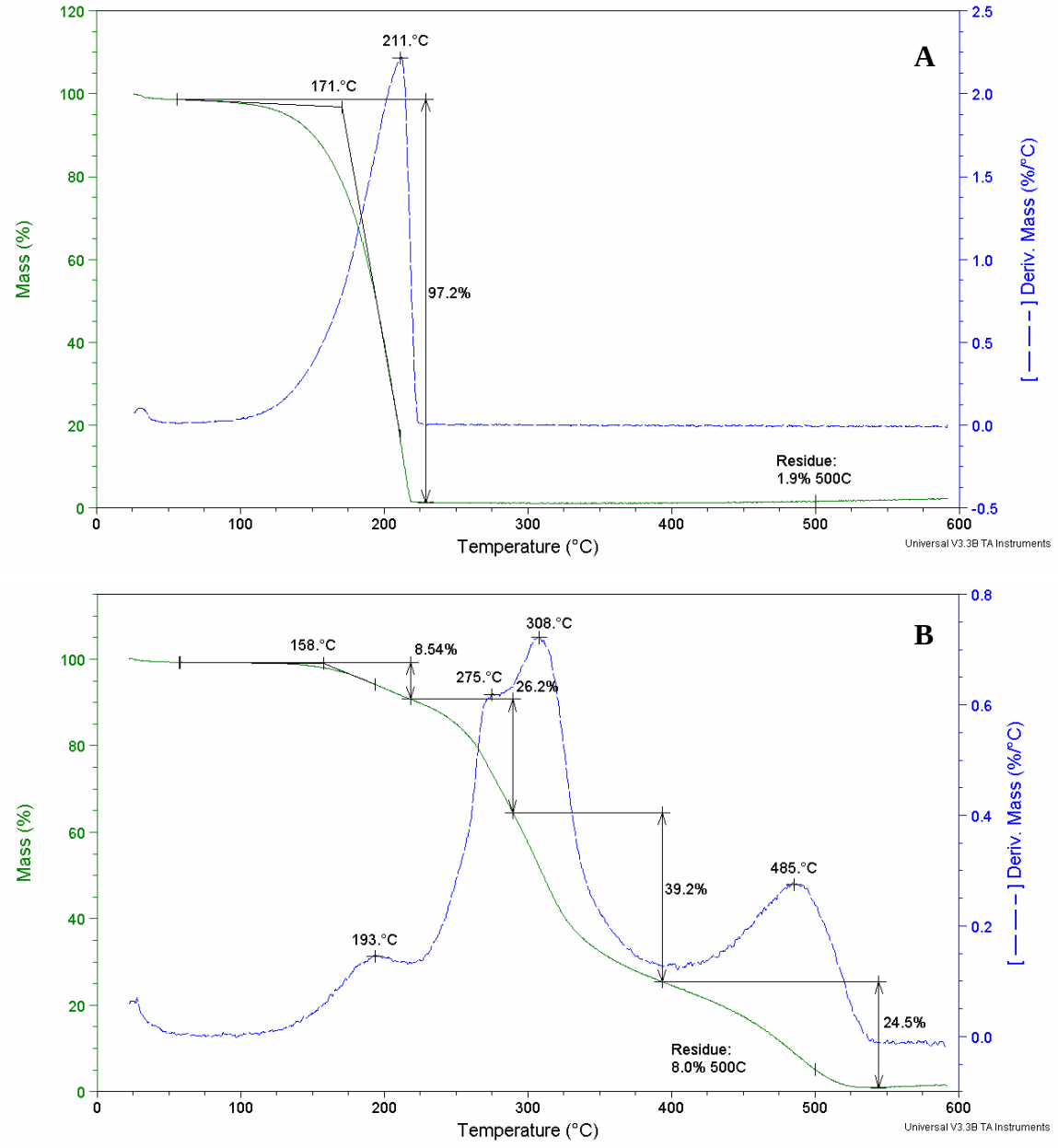

Figure 4.1 TPS 20 (A) and SLO (B) thermo-oxidative decomposition profiles by TGA.

Table 4.2 Summary of TGA thermo-oxidative decomposition data for the sulfurised EP additives. Errors are less than ± 10 % for all measurements except the % residue at 500 ^{o}C (± 20 %).

Additive	T_{onset} (^{o}C)	T_{max} Event 1 (^{o}C)	Mass Loss Event 1 (%)	T_{max} Event 2 (^{o}C)	Mass Loss Event 2 (%)	T_{max} Event 3 (^{o}C)	Mass Loss Event 3 (%)	T_{max} Event 4 (^{o}C)	Mass Loss Event 4 (%)	T_{max} Event 5 (^{o}C)	Mass Loss Event 5 (%)	% Residue at 500 ^{o}C
TPS 20	172	213	97.2	-	-	-	-	-	-	-	-	2.1
DAPS	150	184	98.6	-	-	-	-	-	-	-	-	1.7
SLO	158	194	9.40	273	19.3	312*	40.6	-	-	499	29.9	11
SVO	168	215	36.8	248	18.0	292	15.1	338	9.4	477	15.3	6.8

* Event 3 for SLO possibly contains a shoulder at ~ 350 ^{o}C however it is not distinguishable in all three TGA runs.

Despite the low S-S bond dissociation energy associated with the trisulfide bridges contained in TPS 20 (~ 37 kcal mol^{-1}),[5, 20, 21] the initial stages of TPS 20 mass loss are dominated by evaporation. At higher temperatures S-S bond scission, oxidation and reaction with the aluminium pan surface may occur (schemes 1.22, 1.31 and 1.28 in Chapter 1),[1, 3-8, 12, 13, 17-22] accounting for the change in mass loss mechanism after ~ 213 ^{o}C.

S-S bond scission results in the formation of alkylthiyl radicals ($RS^{\bullet}$), which can recombine to form new sulfide linkages,[8, 19-22] adhere to the aluminium pan surface to form thiolates,[4] or abstract hydrogen atoms from the hydrocarbon portion of the additive structure to form alkanethiols and alkyl radicals (schemes 1.27, 1.28 and 1.24 in Chapter 1).[8, 19-22] The alkanethiols formed can subsequently decompose yielding volatile hydrogen sulfide gas (H_2S) and hydrocarbons (scheme 1.25 in Chapter 1), whilst the hydrocarbon radicals can further participate in radical recombination or hydrogen abstraction reactions.[8, 19, 20] Given the relatively low temperatures at which TPS 20 decomposes together with its high C-S bond stability,[20] the evolution of alkenes is negligible (refer to scheme 1.29 in Chapter 1), minimising the formation of branched and/or networked high molecular weight material according to schemes 3.2 and 3.3 in Chapter 3 and leading to the absence of significant amounts of thermally-stable residue.[19, 20]

Oxidation of TPS 20's S-S bonds produces a variety of volatile short-chain and non-volatile high molecular weight species including sulfones, sulfoxides and sulfonic acids.[7, 12, 18] In contrast, reactions between TPS 20's 'active' sulfur bridges and the aluminium pan surface form thermally stable organic aluminium sulfides and/or sulfates (under the oxidising conditions employed, the formation of sulfate species is more probable).[3, 4, 6, 17] The mass loss observed for TPS 20 following the TGA peak maximum is therefore attributable to the evolution of H_2S, volatile short-chain alkanes and sulfurised oxidation species. Accordingly, the 2.1 % residue present at 500 ^{o}C comprises of residual non-volatile decomposition products including high molecular weight sulfur oxides, radical recombination products and organic sulfates.[3, 6] The detection of a such a

limited amount of residue despite the 20 % w/w sulfur contained in the additive structure is consistent with the findings of other researchers;[3, 4, 6] it implies that the application of high pressures - such as those employed during cold rolling – is required to suppress additive evaporation and enable complete conversion of organic sulfur to metal sulfates and/or sulfides.

The SLO thermo-oxidative decomposition profile is more complex, comprising of at least four mass loss events. The onset temperature of mass loss occurs at 158 ^{o}C, 14 ^{o}C lower than for TPS 20 despite the higher molecular weight of the SLO molecule. This is due to residual carbon-carbon double bonds (C=C) present in the SLO alkyl chains lowering SLO's oxidative stability.[23] The first mass loss event observed for SLO (event 1) occurs at a peak temperature of 194 ^{o}C and corresponds to 9.40 % mass loss. Although this level of mass loss approximates the percentage sulfur present in SLO (10 % w/w), event 1 is unlikely to represent the discrete loss of sulfur as this would require C-S bond scission, which is energetically less favourable than S-S bond scission.[5, 19, 20, 22] The presence of C=C bonds in SLO enables the organic alkylthiyl radicals and sulfurised oxidation products formed by S-S bond scission and oxidation to undergo numerous competing reaction pathways, in addition to those described for TPS 20, leading to the formation of volatile and non-volatile products, including:

- reaction with peroxides formed by C=C bond oxidation via recombination and/or redox mechanisms. These reactions give rise to the antioxidant activity of organo-sulfur compounds; [7, 12, 18]
- addition to C=C bonds to form high molecular weight branched and/or crosslinked material (scheme 1.26 in Chapter 1);[21]
- recombination with alkyl or oxygenated radical species formed by C=C oxidation to form sulfurised/oxygenated sulfurised hydrocarbons (scheme 1.27 in Chapter 1),[8, 18-22] and
- C-S bond scission at higher temperatures (scheme 1.29 in Chapter 1) to form sulfur oxides (SO_x) and hydrocarbons (from sulfurised oxidation products) together with various aromatic and cyclised hydrocarbons and sulfur-containing

products (from alkylthiyl radicals).[19, 20, 24]

The event 1 mass loss observed for SLO therefore comprises of evaporation together with the volatilisation of low molecular weight products formed by C=C bond and sulfur oxidation reactions.[18, 19, 25, 26] H_2S evolution may also account for mass loss over this event.[8, 19, 20] The low percentage of sulfur contained in SLO results in low alkylthiyl radical concentrations and $RS^{\bullet}/RS^{\bullet}$ recombination reactions are unfavourable. Instead, processes such as alkylthiyl radical addition to C=C bonds (sourced at lower temperatures from the initial additive structure) and recombination with C=C bond oxidation radicals occur preferentially, generating predominantly high molecular weight and/or non-volatile products.[7, 12, 18, 21]

The second and third mass loss events observed for SLO are superimposed upon one another and occur at average peak temperatures of 273 ^{o}C and 312 ^{o}C respectively. The majority of sample mass (~ 60.0 %) is converted to volatiles during these events, although the proportions of mass loss that can be attributed to each varies between TGA runs, suggesting an interdependency of the reactions giving rise to mass loss. At the higher event 2 temperatures C-S bond scission can occur, resulting in the formation of alkenes[19, 20] and promoting the evolution of oxygenated radical species which can participate in the decomposition, recombination and polymerisation reactions described in Chapter 3.1[23, 25, 26] or undergo redox reactions with oxidised sulfur species to form alcohols.[7, 12, 18] The higher concentration of unsaturates also favours alkylthiyl radical addition to C=C bonds, increasing the formation of high molecular weight material containing sulfide linkages.[21] Other sulfur-containing functional groups in the SLO structure may also decompose at higher temperatures; the thermolysis of thiiranes to yield alkenes and S_2 is well-documented within the event 2 temperature range (scheme 1.30 in Chapter 1).[20] Furthermore, the formation of sulfur-containing cyclic and benzene-type derivatives is probable.[19, 20, 24] Although these reaction pathways evolve volatile species (H_2S, short-chain carbonyls and alkanes) and give rise to the ~ 19.3 % sample mass loss observed during event 2, they also produce considerable amounts of thermally stable branched and/or crosslinked materials.

Event 3 (T_{max} = 312 ^{o}C) represents the more significant proportion of SLO mass loss at ~ 40.6 %, suggesting it corresponds to the decomposition and volatilisation of products formed during events 1–2. Further decomposition of residual oxygenated or sulfurated radical species is likely to occur, as is the oxidation of remaining sulfides.[7, 12, 18]

The final mass loss event (event 5) occurs at an average peak temperature of 499 ^{o}C, corresponds to ~ 29.9 % mass loss and represents the decomposition of thermally stable deposits remaining after event 3.[27, 28] This level of mass loss is more significant and occurs at higher peak temperature than the final mass loss events observed for triglycerides in Chapter 3.2 (T_{max} for the final triglyceride mass loss event occurs in the range 477-486 ^{o}C and corresponds to 5.89-18.1 % mass loss), inferring that the deposits formed by SLO during events 2 and 3 are more thermally stable than the crosslinked/branched deposits formed by polymerisation of unsaturated hydrocarbons.[7] Accordingly, SLO leaves a large amount of residue at 500 ^{o}C (11.0 %) and its decomposition end temperature (551 ^{o}C) is ~ 50 ^{o}C above the average temperature employed during the continuous annealing process.

The thermo-oxidative decomposition of SVO is analogous to that of SLO, however the temperatures at which mass loss events occur and the corresponding proportions of mass loss vary considerably (see table 4.2). These differences flow from variations in the chemical structures of the sulfurised triglycerides. Vegetable oils generally contain higher levels of unsaturated fatty acid alkyl chains than lard oil.[23] However, SVO's mass loss onset temperature and event 1 peak temperature are 21 ^{o}C and 10 ^{o}C higher respectively than those measured for SLO implying that SVO is more resistant to thermo-oxidative decomposition. Given that SLO and SVO both contain 10 % w/w 'inactive' sulfur,[13] this increased thermo-oxidative stability suggests that the sulfur bridges in SVO are of shorter average chain length than those in SLO[2, 5] and is consistent with C=C bonds in the triglyceride starting material being almost entirely reacted.

Higher concentrations of alkylthiyl radicals and low molecular weight products are therefore formed via S-S bond scission and oxidation respectively by SVO

decomposition during event 1. These conditions, combined with the higher temperature at which event 1 occurs, favour the formation of volatile compounds such as alkanethiols and short-chain hydrocarbons/radical recombination products,[8, 19, 20] contributing to the high proportion of SVO event 1 mass loss (~ 36.8 %). As a result, SVO forms less high molecular weight material over events 1 and 2 and its event 3–5 peak temperatures/mass losses are significantly lower than for SLO; SVO loses approximately half as much mass over event 5 (15.3 %), leaves only 6.8 % residue at 500 ^{o}C and is completely decomposed by ~ 535 ^{o}C.

DAPS contains a high level of 'active' sulfur (~ 38 % w/w) in the predominant form of pentasulfide bridges between its hydrocarbon chains. Its thermo-oxidative decomposition profile is similar to that of TPS 20; it decomposes via a single mass loss event with an onset point of 150 ^{o}C and a peak temperature of 184 ^{o}C. These values are lower than for any of the other sulfurised additives due to the low molecular weight of the DAPS molecule and the greater reactivity of its pentasulfide chains.[2, 5, 19, 20] DAPS therefore undergoes less evaporation than TPS 20 prior to thermo-oxidative decomposition; only 67 % mass loss occurs before the maximum peak temperature is reached. The greater volatility of DAPS results in the availability of less high molecular weight residue-forming reactants (such as alkenes) at higher temperatures and lowers its decomposition end temperature (~ 215 ^{o}C) and % residue at 500 ^{o}C (1.7 %) in comparison to TPS 20.

4.1.3.1.2 PDSC

Figure 4.2 shows an overlay of the heat flow vs. temperature plots obtained for the four sulfurised additives by constant-volume PDSC analysis. Table 4.3 summarises the onset point (T_{onset}), peak and shoulder temperature ($T_{max)}$ and respective enthalpy values determined from the curves.

The PDSC thermo-oxidative decomposition profiles obtained for SLO and SVO mimic their respective DTG curves and at least four exothermic events are observed between room temperature and 500 ^{o}C. The PDSC onset points of oxidation measured for SLO

and SVO are similar at 214 ^{o}C and 209 ^{o}C respectively. These values are ~ 50 ^{o}C higher than the corresponding TGA onset points of mass loss (158 ^{o}C and 168 ^{o}C), confirming the evaporative nature of the initial stages of sulfurised triglyceride mass loss.

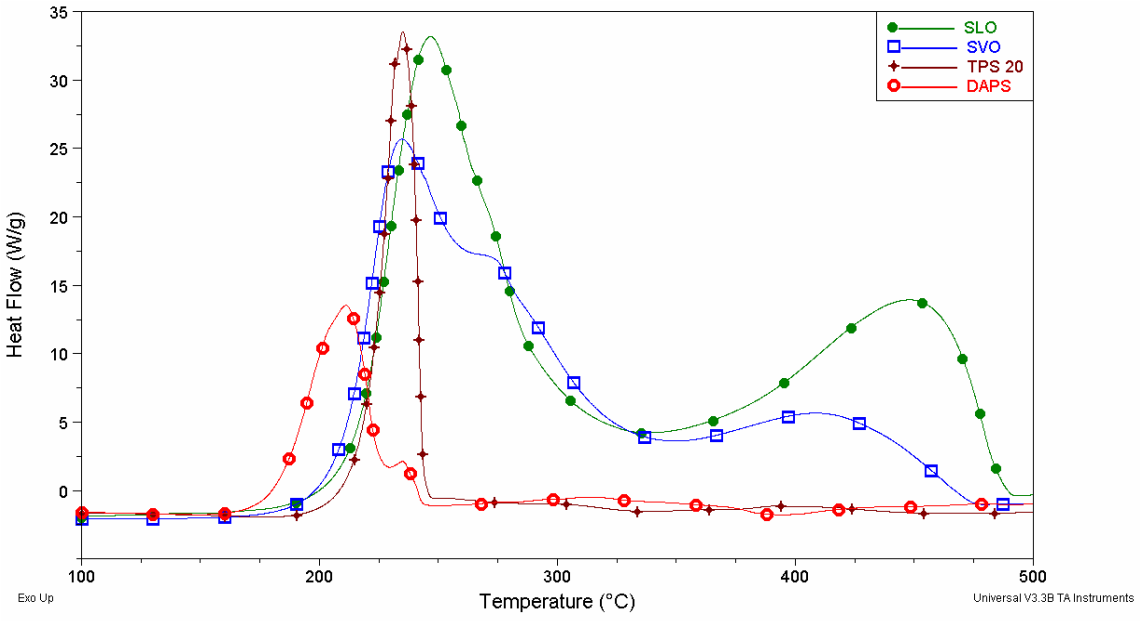

Figure 4.2 Overlay of the sulfurised additive PDSC thermo-oxidative decomposition profiles.

The first of the four overlapping exotherms observed for the sulfurised triglycerides occurs at a peak temperature of 246 ^{o}C in SLO and corresponds to ~ 34 % of the total heat flow. This exotherm represents a combination of exothermic and endothermic processes including S-S bond scission (endothermic) and oxidation (exothermic), together with the oxidation of C=C bonds present in the SLO alkyl chains (exothermic). As determined by Sundarrajan et al.[24] for several unsaturated polysulfide polymers, the total enthalpy associated with this first event is exothermic, indicating that the oxidative processes outlined above are dominant. In SVO, exotherm 1 occurs at ~ 235 ^{o}C (11 ^{o}C lower than in SLO) and corresponds to a greater proportion of the total heat flow (41 %) as a result of the larger number of S-S bonds available to undergo reaction.

Table 4.3 Summary of PDSC data for the sulfurised EP additives. Errors are less than ± 10 % for all measurements except the enthalpy of exotherm 4/the 'tail-like' decomposition region (± 20 %).

Additive	T_{onset} oxidation (^oC)	Exotherm 1		Exotherm 2		Exotherm 3		Exotherm 4 (SLO, SVO) Tail-Like Region (DAPS, TPS 20)	
		T_{max} (^oC)	ΔH (J g^{-1})	T_{max} (^oC)	ΔH (J g^{-1})	T_{max} (^oC)	ΔH (J g^{-1})	T_{max} (^oC)	ΔH (J g^{-1})
TPS 20	220	233	3470	-	-	-	-	376	532
DAPS	182	212	3100	235	286	-	-	301	729
SLO	214	246	7480	268	2560	290	2450	460	9720
SVO	209	235	6620	268	2050	285	3550	409	3800

Exotherm 2 occurs at 268 ^{o}C in both sulfurised triglycerides and indicates the commencement of C-S scission reactions, the reactions of already-formed alkylthiyl radicals and further decomposition of sulfur-containing groups such as thiiranes.[19, 20] As previously discussed, these processes give rise to the formation of a range of cyclic, aromatic and unsaturated decomposition products.[8, 19, 20, 24] Unlike exotherm 1, exotherm 2 corresponds to approximately the same fraction of the total heat flow in SLO and SVO (12 % and 13 % respectively), indicating that similar proportions of the above reactions occur in the two additives.

Although difficult to distinguish, exotherm 3 occurs at roughly the same temperature in SLO and SVO (290 ^{o}C and 285 ^{o}C respectively). It accounts for twice as much of the total heat flow in SVO (22 %) as in SLO (11 %) as a result of the exothermic and endothermic processes it represents; evaporation and thermo-oxidative decomposition of products formed at lower temperature, oxidation of residual organosulfides and recombination and/or decomposition of remaining radical species. Evaporation, an endothermic process, is likely to play a greater role in the decomposition of SLO, accounting for its lower proportion of total heat flow represented by exotherm 3. This is in agreement with observations made by TGA; SLO loses more than twice as much mass as SVO over the corresponding TGA mass loss event (event 3).

Exotherm 4 consumes the entire 'tail-like decomposition region' for SLO and SVO and signifies the thermal cracking and oxidative decomposition of thermally stable deposits formed at lower temperatures.[27, 28] SLO's exotherm 4 peak temperature (460 ^{o}C) is ~ 50 ^{o}C higher than that measured for SVO (409 ^{o}C) and the enthalpy associated with exotherm 4 corresponds to 24 % and 44 % of the total heat flow for SVO and SLO respectively. These observations affirm that in comparison to SVO, SLO thermo-oxidatively decomposes to form a more significant amount of high molecular weight branched and/or crosslinked material and that this material is considerably more thermally stable.

The TPS 20 and DAPS PDSC thermo-oxidative decomposition profiles also emulate their respective DTG curves. However, the results are notably different to the PDSC

profiles of the sulfurised triglycerides with exotherm 1 representing more than 75 % of the total heat flow for DAPS and 87 % of the total heat flow for TPS 20. TPS 20 is considerably more resistant to oxidation than DAPS and either of the two sulfurised triglycerides, exhibiting an oxidation onset temperature of 220^{o}C (T_{onset} DAPS = 182 ^{o}C). This is consistent with the findings of others[5, 12, 20] and is due to factors described previously together with the symmetry and lack of immediate branching on the aliphatic alkyl chains present in TPS 20[19, 20] and the sulfur in TPS 20 being present as aliphatic sulfur bridges (in SVO and SLO some sulfur is present in the form of thiirane functional groups, which are less thermally stable).[20]

As for the sulfurised triglycerides, the TPS 20 PDSC oxidation onset temperature is ~ 50 ^{o}C higher than its onset temperature of mass loss by TGA (172 ^{o}C). In contrast, the PDSC T_{onset} value measured for DAPS is only 30 ^{o}C above its TGA onset of mass loss (150 ^{o}C), evidencing the enhanced reactivity of DAPS' pentasulfide bridges.[5, 20]

Exotherm 1 for TPS 20 occurs at a peak maximum of 233 ^{o}C and its sharp profile is typical of rapid oxidation and combustion-type reactions.[29] It is followed by a tail-like decomposition region (> 250 ^{o}C) comprising of multiple exothermic and endothermic events (T_{max} = 376 ^{o}C, ΔH = 532 J g^{-1}, 13 % of total heat flow) that represent the decomposition and volatilisation of residual carbonaceous material and the formation of sulfate/sulfide deposits.[3, 6, 17, 27, 28, 30] On the contrary, DAPS displays two exothermic events below 250 ^{o}C; exotherm 1 occurs at ~ 212 ^{o}C and exotherm 2 at 235 ^{o}C. Both exotherms are broad in appearance, however their total enthalpy (~ 3390 J g^{-1}, or 82 % of total heat flow) approximates that of exotherm 1 in TPS 20. These differences once again reflect the high reactivity of DAPS; a greater proportion of volatile sulfurised oxidation products are formed at low temperatures and less material is present at higher temperatures to undergo subsequent decomposition reactions. Despite this, DAPS exhibits more heat flow over the tail-like region (729 J g^{-1} or 18 % of total heat flow) than TPS 20. This additional heat flow is not associated with a significant amount of TGA mass loss and is unlikely to indicate oxidation/combustion of residual carbonaceous or sulfur-based deposits. Taking into account the high level of surface-

active sulfur contained in DAPS (~ 38 % w/w), the tail-like region could signify the formation of greater amounts of metal sulfates/sulfides. This appears to contradict the TGA % residue results, which show that less residue is present at 500 ^{o}C for DAPS (1.7 %) than for TPS 20 (2.1 %). However, the two observations can be reconciled if the TPS 20 residue comprises of a greater amount of carbonaceous material than for DAPS.

4.1.3.2 Thermo-Reductive Decomposition Profile

4.1.3.2.1 TGA

TGA analysis of the sulfurised additives under HNX affords the thermo-reductive decomposition profiles (DTG curves) in figure 4.3. A summary of the onset points (T_{onset}), peak temperatures (T_{max}) and relevant mass losses is presented in table 4.4.

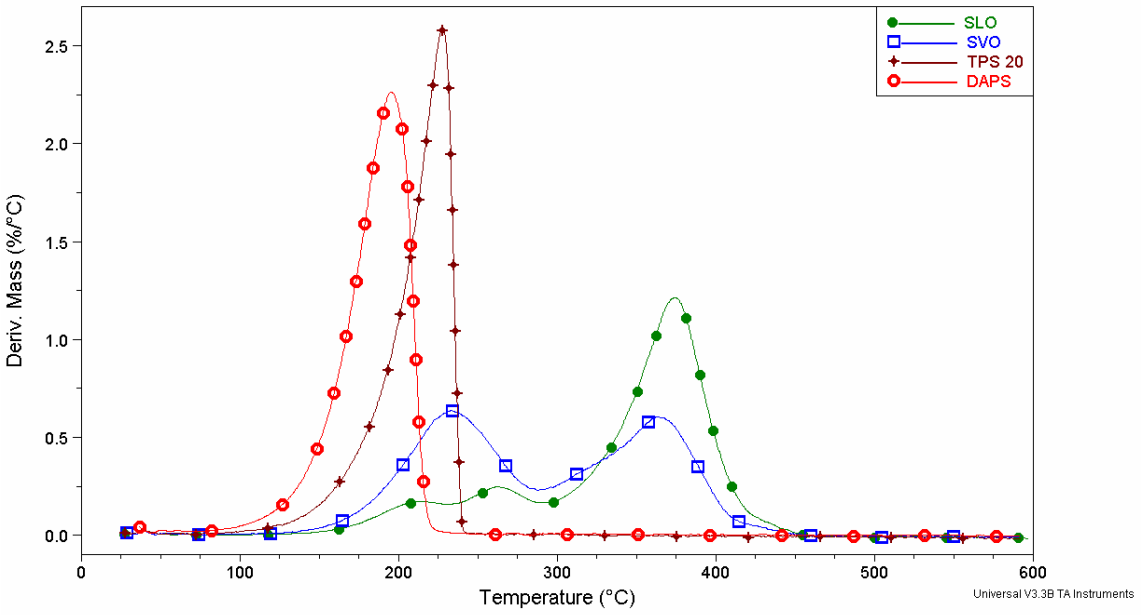

Figure 4.3 Overlay of the TGA thermo-reductive decomposition profiles (DTG curves) of the sulfurised EP additives.

The thermo-reductive decomposition profiles of TPS 20 and DAPS are analogous to those under oxygen and consist of a single event accounting for ~ 97.6 % mass loss.

Despite this similarity, the stability of the two additives is greater under HNX than under oxygen. The thermo-reductive onset and peak temperatures measured for TPS 20 (T_{onset} = 189 ^{o}C; T_{max} = 227 ^{o}C) are 17 ^{o}C and 14 ^{o}C higher than the corresponding values measured under oxygen (T_{onset} = 172 ^{o}C; T_{max} = 213 ^{o}C). Similarly, the onset and peak temperature values measured for DAPS under HNX (T_{onset} = 162 ^{o}C; T_{max} = 197 ^{o}C) are 12 ^{o}C and 13 ^{o}C higher than the analogous thermo-oxidative values (T_{onset} = 150 ^{o}C; T_{max} = 184 ^{o}C). This increased thermal stability can be rationalised by considering the processes giving rise to sample mass loss under HNX. S-S bond oxidation reactions are precluded under thermo-reductive conditions so that evaporation and S-S bond scission are the primary volatilisation processes. In addition to the reaction pathways available under oxygen, the alkylthiyl radicals formed under thermo-reductive conditions can react with gaseous hydrogen to form alkanethiols according to scheme 4.1.[30, 31]

$$2RS^{\bullet}_{(l)} + H_{2(g)} \rightarrow 2RSH_{(g)}$$

Scheme 4.1 Reaction of alkylthiyl radicals with gaseous hydrogen to form alkanethiols.

Alkanethiol formation is therefore a favourable route for the consumption of alkylthiyl radicals under HNX so that a greater proportion of additive mass loss occurs via alkanethiol evaporation and decomposition.[19, 20] The higher thermo-reductive onset and peak temperature values measured for DAPS and TPS 20 therefore result from a lack of oxidative decomposition and the greater role played by evaporation during the initial stages of mass loss. The levels of residue remaining at 500 ^{o}C after the thermo-reductive decomposition of DAPS and TPS 20 are similar to the values determined under oxidising conditions (~ 2 %). In accordance with the findings of Riga et al.,[17] the composition of this residue is likely to be aluminium sulfate-based.

The sulfurised triglycerides also exhibit greater stability under HNX; the thermo-reductive onset and event 1 peak temperature values measured for SLO (T_{onset} = 177 ^{o}C; T_{max} = 211 ^{o}C) are 19 ^{o}C and 17 ^{o}C higher than the corresponding values measured

under oxygen (T_{onset} = 158 ^{o}C; T_{max} = 194 ^{o}C). Similarly, the onset and event 1 peak temperatures measured for SVO under HNX (T_{onset} = 186 ^{o}C; T_{max} = 228 ^{o}C) are 18 ^{o}C and 13 ^{o}C higher than the values measured under oxygen (T_{onset} = 168 ^{o}C; T_{max} = 215 ^{o}C). As for the sulfurised hydrocarbons, the lack of oxygen prevents S-S bond oxidation reactions from occurring, accounting for the observed increase in onset temperature and event 1 peak temperature.

Table 4.4 Summary of TGA thermo-reductive decomposition data for the sulfurised EP additives. Errors are less than ± 5 %.

Additive	T_{onset} (^{o}C)	T_{max} Peak 1 (^{o}C)	Mass Loss Peak 1 (%)	T_{max} Peak 2 (^{o}C)	Mass Loss Peak 2 (%)	T_{max} Peak 3 (^{o}C)	Mass Loss Peak 3 (%)	% Residue at 500 ^{o}C
TPS 20	189	227	97.6	-	-	-	-	2.4
DAPS	162	197	97.6	-	-	-	-	2.1
SLO	177	211	10.1	263	11.8	372	74.4	3.4
SVO	186	228	48.5	-	-	359	46.5	4.8

However, the use of thermo-reductive conditions has a two-fold effect on the stability of SLO and SVO; oxidation of C=C bonds in the sulfurised triglyceride structures is also precluded so that the overall increase in low-temperature stability is greater than for the sulfurised hydrocarbons and is greater for SLO (which contains more C=C bonds) than for SVO.[23]

The first thermo-reductive mass loss event (event 1) observed for the sulfurised triglycerides corresponds to 10.1 % and 48.5 % mass loss for SLO and SVO respectively. These levels of mass loss are higher than those measured for event 1 under

thermo-oxidising conditions (9.40 % and 36.8 % for SLO and SVO). As outlined for DAPS and TPS 20, alkanethiol formation via scheme 4.1 and reactions between alkylthiyl radicals and saturated portions of the additive structure are prolific. These reactions lead to the formation of high levels of volatiles and result in the greater amount of thermo-reductive event 1 mass loss observed for SLO and SVO.[8, 19, 20, 30, 31] Unlike the sulfurised hydrocarbons, a third route for alkanethiol formation is available in SLO and SVO; the presence of C=C bonds enables mono allylic hydrogen abstraction to occur.[21] This creates alkyl radicals that can react in the same manner as the oxygenated radicals ($RO^{\bullet}$, $ROO^{\bullet}$) formed under oxidising conditions to create high molecular weight branched and/or crosslinked material.[25, 26] However, the extent of branching and crosslinking reactions undergone by alkyl radicals is limited by the presence of gaseous hydrogen, which can quench the propagating radicals via the analogous reaction to scheme 4.1 above ($RS^{\bullet}$ is replaced by $R^{\bullet}$). Similarly, alkylthiyl radicals formed by S-S bond scission can add to C=C bonds and form high molecular weight material containing sulfide linkages, however this material possesses inferior thermal stability as it is susceptible to decomposition via S-S bond scission.[21] Therefore, under thermo-reductive conditions, high levels of mass loss are observed over event 1 for SLO and SVO although the high molecular weight deposits formed are structurally similar to those formed under an oxidising environment.

Event 2 for the sulfurised triglycerides also occurs at lower temperature under HNX (T_{max} = 263 ^{o}C for SLO, 10 ^{o}C lower than under oxygen) and is superimposed upon event 1 for SVO. The processes giving rise to event 2 mass loss under HNX are similar to those that occur in an oxygen environment; large amounts of alkenes and cyclics are formed via C-S bond scission.[19, 20, 24] Alkene oxidation is once again precluded.

The high-temperature mass loss profiles displayed by the sulfurised triglycerides under HNX differ significantly to those under oxygen. Whilst three thermo-oxidative mass loss events in the range 290-500 ^{o}C give rise to a total of 70.5 % and 39.8 % mass loss for SLO and SVO respectively, under HNX a single mass loss event (event 3) occurs in the range 359-372 ^{o}C, corresponding to 74.4 % (SLO) and 44.4 % (SVO) mass loss.

Although these results show that a more significant amount of high-temperature thermo-reductive mass loss occurs for the sulfurised triglycerides, the thermal stability of the residue giving rise to this mass loss is lower than that of the corresponding residue formed under oxygen. Accordingly, the thermo-reductive decomposition end temperatures measured for SLO and SVO (T_{end} = 460 ^{o}C) under HNX are 91 ^{o}C and 75 ^{o}C below the corresponding thermo-oxidative T_{end} values (551 ^{o}C and 535 ^{o}C respectively). The residue remaining at 500 ^{o}C after decomposition of SLO and SVO under HNX is also considerably lower than under oxygen, at only 3.4 % (SLO) and 4.8 % (SVO). This is in agreement with Sech and Oleksiak,[13] who noted that the addition of sulfurised fat to cold rolling oil lowers residue levels after thermo-reductive decomposition. HNX therefore promotes effective sulfurised EP additive volatilisation and minimises the formation of thermally stable residues that can compromise metallic coating quality.

4.1.3.3 Characterisation of Decomposition Reactions by Mid-Infrared and Far-Infrared Techniques

4.1.3.3.1 Mid-Infrared ATR Analysis

Figure 4.4 shows the mid-infrared ATR spectra obtained for DAPS, TPS 20 and SVO at room temperature. The room temperature spectrum of SVO is representative of that obtained for SLO. The peak assignments for these spectra are given in table 4.5.

The spectra collected for SLO and SVO show similar features. A weak band at ~ 3002 cm^{-1} indicates that the additives contain small amounts of unreacted C=C bonds[32] and some free fatty acids are likely to be present, as indicated by a weak O-H stretching band at 3479-3461 cm^{-1} and a C=O stretching band at 1710 cm^{-1}. Evidence of the thiocarbonyl group is present in the form of several characteristic bands in the fingerprint region (1400-600 cm^{-1}).[32]

The unsaturated C-H (> 3000 cm^{-1}) and C=O (1750-1700 cm^{-1}) stretching bands found in the sulfurised triglyceride spectra are absent in the spectra of TPS 20 and DAPS, confirming that DAPS and TPS 20 contain saturated, hydrocarbon-based alkyl chains.

Numerous peaks characteristic of *tert* butyl and sulfur-containing functional groups are present in the fingerprint region for both sulfurised hydrocarbons. Strong absorptions in the DAPS spectrum at 1470 cm^{-1} and 1445 cm^{-1}, together with a weak absorption at 1315 cm^{-1}, are assigned to CH_3-S asymmetrical and symmetrical stretching vibrations and suggest the presence of R-S-CH_3 groups.[33] These bands are absent in the TPS 20 spectrum; long dodecyl alkyl chains are attached to TPS 20's sulfur bridges.

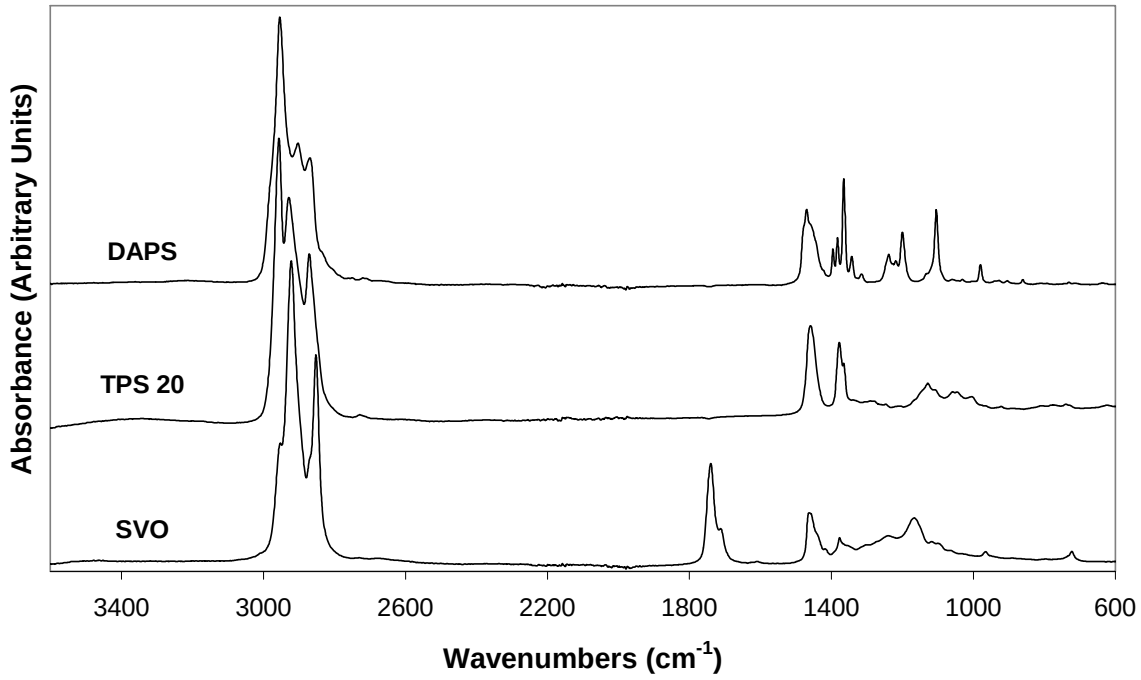

Figure 4.4 Mid-IR ATR spectra of DAPS, TPS 20 and SVO acquired at room temperature.

Evidence of sulfur chain oxidation, even at room temperature, is present for both DAPS and TPS 20; a weak absorption at 1343-1339 cm^{-1} is assigned to symmetrical S=O stretching in sulfones.[32, 34] Oxidation is not observed for the sulfurised triglycerides as their shorter sulfur chains possess greater oxidative stability.[5, 19, 20] Several weak absorptions at 1045-1031 cm^{-1}, 1061-1058 cm^{-1} and 1131-1129 cm^{-1} are also indicative of sulfur oxidation products,[32, 34, 35] however they could alternatively be due to the thiocarbonyl group.[32, 34]

Table 4.5 Peak assignments for the sulfurised EP additive room temperature ATR spectra.[32, 34, 36]

Peak (cm^{-1})				Assignment
DAPS	**TPS 20**	**SVO**	**SLO**	
-	3341	3461	3479	νO-H in COOH; νO-H in SO_3H
-	-	3002	3002	νC-H (unsaturated)
2954	2956	2952	2953	νC-H in $–CH_3$ (asym.)
-	2928	2921	2921	νC-H in $–CH_2$- (asym.)
2903	-	-	-	νC-H in $–CH_3$ (sym.)
2869	2871	2852	2850	νC-H in $–CH_2$- (sym.)
-	-	1740	1738	νC=O in RCOOR
-	-	1712	1710	νC=O in COOH
1470	-	-	-	γC-H in CH_2/CH_3; δMe-S in R-S-CH_3 (asym.)
1458	1459	1463	1465	
1445	-	-	-	
1395	-	-	-	γC-H in $–C(CH_3)_3$ (asym.)
1383	1378	1377	1378	γ-CH_3 (sym.)
1365	1365	-	-	γC-H in $–C(CH_3)_3$ (sym.)
1343	1339	-	-	νS=O in -SO_2- (asym.); νS=O in SO_3H (asym.)
1315	-	-	-	νS=O in -SO_2- (asym.); δMe-S in R-S-CH_3 (sym.)
1238	1247	1240	1235	νC-O (esters); -C-$(CH_3)_3$ skeletal vibration
1219	-	-	-	-C-$(CH_3)_3$ skeletal vibration
1200	-	-	-	νC=S; -C-$(CH_3)_3$ skeletal vibration
-	-	1170	1180	νC=S; νC-O in RCOOR
1131	1129	-	-	νC=S; νS=O in -SO_2- (sym.)
-	-	1118	1115	νC-O in RCOOR; νC=S
1104	1106	1101	1101	νC=S; νC-O in RCOOR
1061	1058	-	-	νC=S; νS=O in –SO-
1031	1045	-	-	
-	-	966	966	γC-H in *trans* -CH=CH-
731	739	723	718	$(CH_2)_n$ rocking; γC-H in *cis* -CH=CH-

ν = stretching; δ = bending; γ = out-of-plane deformation

asym. = asymmetrical; sym. = symmetrical

Since DAPS does not contain any carbonyl or hydroxyl moieties, a strong, sharp band present in its spectrum at 1104 cm^{-1} confirms the presence of C=S.[32] The corresponding absorption at 1106 cm^{-1} in TPS 20 is much weaker and broader and could result from alcohol contaminants. This is supported by the presence of a broad O-H stretching absorption in the TPS 20 spectrum at 3341 cm^{-1}.[32, 34] Both DAPS and TPS 20 display several sharp, intense absorptions which are typical of the *tert* butyl group. [34, 36]

The bands at 1101 cm^{-1}, 1118-1115 cm^{-1} and 1180-1170 cm^{-1} can therefore be monitored during the sulfurised triglyceride thermo-oxidative decomposition process to detect the volatilisation and/or reaction of the thiocarbonyl group present in the additive structure. Although there are no distinctive bands associated with the 'inactive' sulfur chains present in SLO and SVO, the regions at ~ 3030 cm^{-1} and 1420-1030 cm^{-1} can be used to identify the build up of sulfurised degradation products such as sulfur-containing cyclics, aromatics and oxides respectively[20, 24, 32, 34] and the formation of metal carboxylates can be detected by the emergence of bands in the region 1650-1300 cm^{-1}.[37-39] The build-up of oxygenated decomposition products and degradation of aliphatic hydrocarbon chains has been described in detail for triglycerides in Chapter 3.2 and will not be dealt with extensively in this Chapter.

Figure 4.5 shows the ATR spectra obtained for thermo-oxidatively decomposed TPS 20 and SVO in the temperature range 100-350 ^{o}C in the C=O stretching/fingerprint region (1920-1000 cm^{-1}). The spectra acquired for DAPS and SLO are analogous. Table 4.6 provides a comparative summary of the thermo-oxidative decomposition steps undergone by all four additives.

For TPS 20, a gradual decrease in spectral intensity is observed until ~ 150 ^{o}C, showing that the mass loss process below this temperature is dominated by evaporation. Between 100-150 ^{o}C, the bands at 1058 cm^{-1} and 1045 cm^{-1} disappear. The high volatility of the moieties giving rise to these absorptions supports the assignment of these bands to sulfoxide S=O stretching in table 4.5. The unchanged intensity of the band at 1128 cm^{-1} indicates that the oxidation products formed are at least partially non-volatile in nature.[18] At 215-230 ^{o}C new bands typical of S=O stretching in sulfones (1327 cm^{-1}) and sulfonic

acids (1351 cm^{-1}) appear,[32, 34, 35] signifying TPS 20 sulfur bridge oxidation.[7, 12, 18]

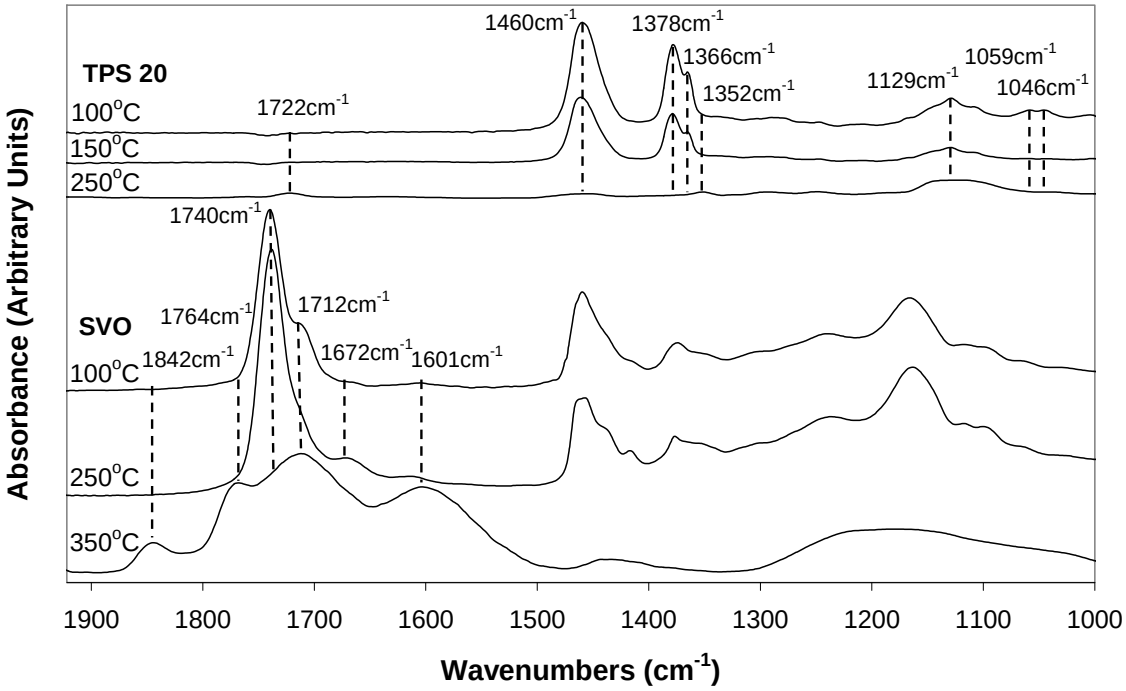

Figure 4.5 Mid-IR ATR spectra of thermo-oxidatively decomposed TPS 20 and SVO in the region 1920-1000 cm^{-1}.

Numerous transformations in the carbonyl and fingerprint regions are apparent at 250 °C. Broadening of the 1128 cm^{-1} band (S=O symmetrical stretching in sulfones) occurs and there is no decrease in its intensity. The sulfonic acid and sulfoxide bands increase in intensity, indicating that non-volatile sulfurised oxidation products continue to be evolved. The appearance of an absorption at 1722 cm^{-1} suggests that carboxyl-containing compounds are produced,[32] most likely as a result of C-S bond scission and the subsequent formation and oxidation of unsaturated species.[19, 20, 25, 26] The evolution of broad shoulders on the ~ 1352 cm^{-1} band in the range 1410-1385 cm^{-1} and on the ~ 1121 cm^{-1} band in the range 1210-1170 cm^{-1} implies that organic sulfates are also produced.[34]

Table 4.6 Summary of the temperatures at which spectral changes are observed for the sulfurised EP additives. The observed changes are assigned to specific thermo-oxidative decomposition processes.

Spectral Change	Decomposition Process	Temperature Range (°C)			
		SLO	SVO	DAPS	TPS 20
Decrease in spectral intensity	Evaporation of volatile fatty acids & sulfur oxides	150-250	RT-200	RT-150	RT-150
Disappearance of 3002 cm^{-1} band	Consumption of C=C (polymerisation)	200-250	200-250	N/A	N/A
Shift in 1470 cm^{-1} band to lower wavenumber	Degradation of sulfur-methyl group	N/A	N/A	150-200	N/A
Evolution of 1609 cm^{-1} band	Formation of metal carboxylates	250-300	200-350	N/A	N/A
Evolution/broadening/shift/increase in absorption of 1360-950 cm^{-1} bands	Detection & build up of sulfurised oxidation products (sulfoxides, sulfones, sulfonic acids, sulfonates, sulfates)	350-450	300-400	150-205	200-250
Evolution of 1410-1375 cm^{-1} & 1210-1160 cm^{-1} bands	Formation of organic sulfates	350-400	300-350	200-215	230-250
Evolution of 1725-1672 cm^{-1} bands	C-S scission & oxidation (carboxyl-containing compounds)	300-350	200-250	200-215	230-250
Appearance & increased intensity of 817-714 cm^{-1}, 3093 cm^{-1} & 1520 cm^{-1} bands	C-S scission & back-biting (cyclic and benzene-type species)	300-400	200-300	150-200	N/A
Disappearance of bands in νC-H region	Complete hydrocarbon chain decomposition	400-450	350-400	205-230	250-300
No spectral absorption	Complete residue decomposition	>500	>500	~230	~300

This is in agreement with the findings of Komvopoulos et al.[6] and Najman et al.,[3] who determined that decomposition of sulfurised EP additives on a steel substrate at ~ 100 ^{o}C produces iron sulfates. The higher temperature at which sulfates form on the aluminium pan surface employed in the present study results from the lower catalytic activity of aluminium in comparison to iron.[40] At temperatures above 250 ^{o}C, the intensity of the TPS 20 spectrum decreases significantly and the thermo-oxidative decomposition process is complete at 300 ^{o}C. No persistent sulfate-type residues are detected.

The chemical changes observed during the thermo-oxidative decomposition of DAPS follow the same trend as for TPS 20, however several differences are apparent. Only minor decreases in the intensity of the DAPS spectrum are observed below 150 ^{o}C, indicating a limited amount of additive evaporation. The temperature at which chemical changes to DAPS occur is lower than for TPS 20 (~ 200 ^{o}C, as opposed to 230 ^{o}C) as a result of the high reactivity of the DAPS pentasulfide bridges.[5] The absorptions at 1470 cm^{-1} (C-H deformations in CH_2/CH_3 or methyl-sulfur bending vibration in R-S-CH_3), 1060 cm^{-1} (C=S or sulfoxide S=O stretching) and 1004 cm^{-1} (C=S stretching) are shifted to lower wavenumber (1469 cm^{-1}, 1056 cm^{-1} and 999 cm^{-1} respectively). All three of these bands either represent, in the case of the 1060 cm^{-1} and 1004 cm^{-1} bands, or potentially represent, in the case of the 1470 cm^{-1} band, absorptions due to sulfur-containing species. The fact that the 1470 cm^{-1} band undergoes a change at 200 ^{o}C, whilst the other two bands associated with C-H deformations in CH_2 and CH_3 (at 1458 cm^{-1} and 1445 cm^{-1}) remain unaffected, verifies the assignment of the 1470 cm^{-1} band to methyl-sulfur bending. Although the intensity of the 1470 cm^{-1} and 1004 cm^{-1} bands is relatively unchanged at 200 ^{o}C, that of the 1060 cm^{-1} band increases. This is due to the build up of sulfoxides[32, 34] and demonstrates that the oxidation reactions of sulfur-containing groups in the additive structure commence at this temperature, ~ 30 ^{o}C below the temperature at which analogous products form in TPS 20. The absorption shift to lower wavenumber signifies that these products are of high molecular weight.

The formation of new hydrocarbon structures in DAPS at 200 ^{o}C is supported by the broadening of bands in the C-H stretching (not shown) and *tert* butyl skeletal vibration

regions. In addition, the appearance of an absorption at 714 cm^{-1} implies the formation of benzene-type species.[32] The detection of benzene derivatives is in agreement with the findings reported by Sundarrajan et al.,[24] who determined that benzene, substituted benzenes and a range of cyclised sulfur-containing products are formed by thermal decomposition of saturated and unsaturated polysulfide polymers. Homolytic C-S bond cleavage followed by back-biting by the resultant alkylthiyl radical was proposed as the likely mechanism for the formation of these products. In the present study, no benzene-type compounds are detected during the decomposition of TPS 20; TPS 20 possesses a higher C-S bond dissociation energy than DAPS as discussed previously.[20]

The formation sulfurised oxidation products in DAPS is more pronounced at 205 ^{o}C although, in contrast to TPS 20, a large proportion of these products are volatile (the spectrum decreases significantly in intensity). Disappearance of the band at 714 cm^{-1} indicates volatilisation of benzene species and the build up of carbonyl compounds due to the formation and oxidation of unsaturated species is indicated by a band at 1700 cm^{-1}.[19, 20, 25, 26, 32] Sulfonate esters and organic sulfates are detected via a single, broad absorption at 1375 cm^{-1} and a shoulder on the ~ 1200 cm^{-1} band spanning 1180-1164 cm^{-1}.[32, 34] The DAPS thermo-oxidative decomposition process is complete at temperatures above 230 ^{o}C, ~ 70 ^{o}C below the decomposition end temperature of TPS 20. Once again, persistent organic sulfates are not detectable.

Despite significant support in the literature that alkylthiyl radicals formed during organosulfide decomposition abstract hydrogen to form alkanethiols and alkyl radicals,[8, 19, 20] there is no evidence of alkanethiol formation in either TPS 20 or DAPS; S-H stretching bands in the range 2600-2550 cm^{-1} are absent in the additive spectra.[32] This could be due to the limited concentration any alkanethiol species formed, rapid alkanethiol decomposition into H_2S and alkyl radicals and the poor infrared activity of the S-H functional group.[32]

The mid-IR results obtained for SVO and SLO evidence an entirely different thermo-oxidative decomposition process to that undergone by the hydrocarbon-based additives. This discussion will focus primarily on the results obtained for SVO; the corresponding

changes in SLO are similar and generally occur at higher temperatures.

In contrast to the sulfurised hydrocarbons, SVO undergoes limited evaporation below 200 ^{o}C, although volatilisation of free fatty acids is indicated by a decrease in the C=O stretching absorption at 1712 cm^{-1}. Several chemical changes are apparent, including the consumption of C=C bonds, indicated by the disappearance of the unsaturated C-H stretching band ~ 3002 cm^{-1} (results not shown), and the build up of metal carboxylate species, evidenced by the emergence of a band ~ 1609 cm^{-1}.[32, 34] Metal carboxylates are not observed during the thermo-oxidative decomposition of naturally-occurring triglycerides until ~ 300 ^{o}C and the lower temperature at which metal carboxylates form in SVO and SLO is testament to the high surface activity of sulfurised triglycerides. There is no concurrent build up in hydroxyl species at 200 ^{o}C, inferring that C=C bonds in the additive structure are participating in reactions other than oxidation.

At 250 ^{o}C the carboxylate asymmetrical stretching band at 1609 cm^{-1} is shifted to higher wavenumber (1614 cm^{-1}) and increases in intensity. There is some broadening of the ester C=O stretching band at 1740 cm^{-1} and the peak is shifted to lower wavenumber. A new band characteristic of cyclised carbonyl compounds such as aryl ketones, aldehydes and carboxylic acids emerges in the C=O stretching region at ~ 1672 cm^{-1}.[32] The formation of aromatic decomposition products is also evidenced by the appearance of a C-H stretching band at 3093 cm^{-1}, a broad, aromatic C=C stretching band at ~ 1520 cm^{-1} and bands characteristic of the C-H out-of-plane vibration in various substituted benzenes at 817 cm^{-1} and 747 cm^{-1}.[32] The detection of these compounds suggests the occurrence of C-S bond scission reactions as noted for DAPS.[24]

In contrast to the sulfurised hydrocarbons, SVO shows very little evidence that sulfurised oxidation products are formed below 300 ^{o}C and the detection of such products is complicated by the presence of ester, acid and alcohol absorptions. However, at 300 ^{o}C, carbonyl-type compounds are volatilised and an absorption typical of sulfones, sulfonic acids and sulfonates at 1356 cm^{-1} becomes prominent. A broad S=O stretching band at 1152 cm^{-1} also appears.

More evidence for the formation of sulfurised oxidation products is present at 350 ^{o}C;

broad bands at 1430 cm^{-1} and 1210 cm^{-1} form. The near complete decomposition of the hydrocarbon portion of SVO at this temperature suggests that the 1430 cm^{-1} band is no longer due to C-H out-of-plane deformations in CH_2 and CH_3. Instead, it can be attributed to asymmetrical S=O stretching in organic sulfates.[34] The band formed at 1210 cm^{-1} spans the range 1330-950 cm^{-1} and represents the formation of a variety of sulfones, sulfonic acids, sulfonates and sulfates.[32, 34] The absorption at 1600 cm^{-1}, characteristic of metal carboxylates, increases in intensity. The majority of hydrocarbons are combusted by ~ 450 ^{o}C, however carboxylate, radical recombination and aromatic decomposition products persist at temperatures beyond 500 ^{o}C.

The mid-IR ATR results outlined above augment the data obtained by PDSC and TGA. For DAPS and TPS 20, the lack of chemical changes in spectra collected at low temperatures confirm that the initial stages of TGA mass loss are due to evaporation. Sulfurised oxidation products are first observed at 215-230 ^{o}C for TPS 20 and at ~ 200 ^{o}C for DAPS. These temperatures correspond approximately to the oxidation onset temperatures measured by PDSC (TPS 20 T_{onset} = 220 ^{o}C; DAPS T_{onset} = 182 ^{o}C) and to the event 1 peak maxima measured by TGA (TPS 20 T_{max} = 213 ^{o}C; DAPS T_{max} = 184 ^{o}C), confirming a change in mass loss mechanism from evaporation to thermo-oxidative decomposition.

The mid-infrared changes observed for TPS 20 at temperatures above 230 ^{o}C signify thermal cracking and/or the formation of new hydrocarbon structures, further oxidation of sulfur-containing species and the formation of organic sulfates. These changes correspond to the secondary decomposition region by PDSC and account for very little TGA mass loss; the TGA mass loss end temperature for TPS 20 is ~ 230 ^{o}C. The mid-IR ATR results therefore cannot account for the chemical nature of the 2.1 % TPS 20 residue present at 500 ^{o}C.

For DAPS, sulfurised oxidation products together with aromatic and new hydrocarbon structures formed by C-S bond scission are detected at ~ 200 ^{o}C. These changes correspond to mass loss occurring immediately after the TGA peak maximum (184 ^{o}C) and give rise to the two exothermic events observed for DAPS thermo-oxidative

decomposition by PDSC. The single low-temperature exothermic event observed for TPS 20 equates to the minimal C-S bond scission reaction products that are observed in the TPS 20 spectra. Thermal cracking and further oxidation of DAPS decomposition residues occurs at temperatures above 205 ^{o}C and the temperature at which a significant level of volatilisation is observed by mid-IR (~ 215 ^{o}C) corresponds to the TGA mass loss end temperature (215 ^{o}C).

The first chemical changes in the SVO sample are observed at ~ 200 ^{o}C, and include the loss of free fatty acids, the consumption of C=C bonds and the formation of metal carboxylates. The fact that no hydroperoxides are detected at this temperature evidences the anti-oxidant activity of SVO and suggests that the sulfurised oxidation species which act as peroxide decomposers[18] are formed at lower temperatures (the detection of these species is precluded by absorptions of the triglyceride ester groups). Similarly, the consumption of C=C bonds infers the formation of alkylthiyl radical species as no other reaction pathways are available (C=C bond oxidation is not occurring). These changes correspond to the event 1 peak maximum temperature by TGA (215 ^{o}C) and the onset temperature of oxidation by PDSC (209 ^{o}C).

Carboxylate-type species continue to form at 250 ^{o}C and a range of unsaturates, cyclised carbonyls, benzene derivatives, carboxylic acids and hydroperoxides are detected. The evolution of these products confirms that event 2 by TGA (T_{max} = 248 ^{o}C) and exotherm 2 by PDSC (T_{max} = 268 ^{o}C) represent C-S bond scission and thiirane decomposition, together with the oxidation of C=C bonds. The low level of TGA mass loss (18.0 %) suggests that the majority of the products formed are non-volatile in nature and/or react immediately to form high molecular weight deposits.

SVO volatilisation and the formation of lactones and anhydrides occurs at 300 ^{o}C and implies that event 3 by TGA (T_{max} = 292 ^{o}C; 15.1 % mass loss) and exotherm 3 by PDSC (T_{max} = 285 ^{o}C) involve thermal cracking together with the formation of oxygenated radical recombination products. These reactions continue to occur at 350 ^{o}C and the formation of sulfurised oxidation products and organic sulfates is also apparent. Accordingly, event 4 by TGA (T_{max} = 338 ^{o}C) gives rise to only 9.4 % mass loss,

confirming the non-volatile nature of these materials. At higher temperatures combustion and thermal cracking of residues occurs, corresponding to event 5 by TGA (T_{max} = 477 ^{o}C; 15.3 % mass loss) and exotherm 4 by PDSC (T_{max} = 477 ^{o}C). The presence of residual decomposition products in the SVO spectrum at 500 ^{o}C is in agreement with the high level of residue measured by TGA (6.8 %).

4.1.3.3.2 Far-Infrared ATR Analysis

To gain further insight into the sulfide bridge decomposition process and the chemical nature of residues formed by reactions between the sulfurised additives and the aluminium pan surface, far-IR analysis was performed. The room temperature spectra of DAPS and TPS 20 display absorptions in the far-IR and figure 4.6 shows an overlay of these spectra in the region 600-400 cm^{-1}. Peak assignments are provided in table 4.7.

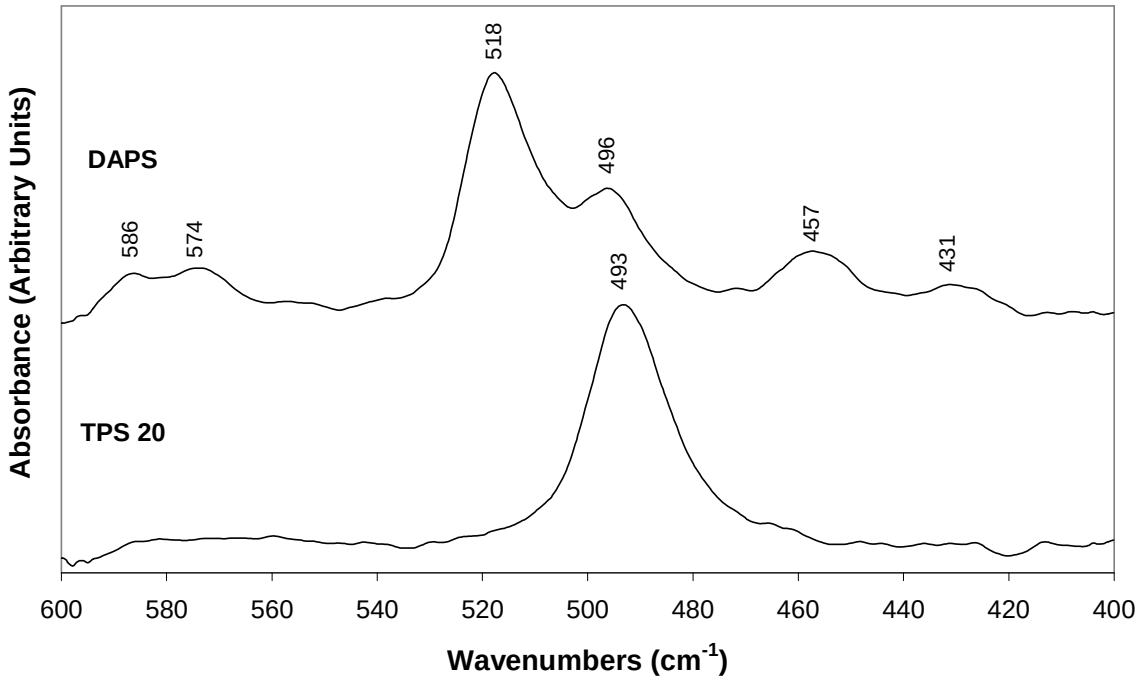

Figure 4.6 Far-IR ATR spectra of DAPS and TPS 20 acquired at room temperature.

The room temperature spectra acquired for SLO and SVO do not display absorptions in

the 600-400 cm^{-1} region, corresponding to the lack of interaction between sulfur groups and the aluminium pan surface and the weak initial adsorption of the ester groups.[13] The TPS 20 spectrum consists of a single band at 493 cm^{-1} representing the sulfide stretching absorption.[41] No bands associated with oxides and hydroxides on the aluminium pan surface are present, which is consistent with the low concentration of such species. Similarly, bands indicative of heterolytic sulfide chain decomposition products (S^-, $[S_2]^-$, $[S_3]^-$) are not detectable, indicating that the trisulfide bridges in TPS 20 are stable at room temperature.

Table 4.7 Peak assignments for DAPS and TPS 20 room temperature far-IR ATR spectra. [41-43]

Peak (cm^{-1})		Assignment
DAPS	**TPS 20**	
586	-	$\nu[S_2]^-$
574	-	$\nu[S_3]^-$; νAl-OH in $Al(OH)_3$
518	-	νS-S
496	493	νS-S
457	-	νS-S; νAl-OH in $Al(OH)_3$
431	-	νS-S; νAl-OH in $Al(OH)_3$

ν = stretching

In contrast, the greater reactivity of the pentasulfide bridges in DAPS give rise to absorptions at 586 cm^{-1} and 574 cm^{-1}, which can be attributed to $[S_2]^-$ and $[S_3]^-$ stretching vibrations respectively.[41] These bands are less intense than the other three absorptions observed in the DAPS spectrum as the majority of the DAPS sample is not decomposed/bonded to the aluminium pan surface. Although the 574 cm^{-1} band could be due to the presence of α-aluminium hydroxide,[42] the fact that no corresponding absorption is observed for TPS 20 (or SLO and SVO) and the greater likelihood of aluminium oxides as opposed to hydroxides being present on the aluminium pan

surface[40] suggests that this assignment is improbable. Similarly, the bands at 457 cm^{-1} and 431 cm^{-1} represent S-S as opposed to Al-OH stretching vibrations.[41, 42] The most intense of the six absorptions occur at 518 cm^{-1} and 496 cm^{-1} and, like the 457 cm^{-1} and 431 cm^{-1} bands, correspond to S-S stretching vibrations.[41, 43] The large number of S-S stretching modes observed for DAPS is consistent with both its long average sulfide chain length and the fact that it contains a distribution of sulfide chain lengths.

By monitoring bands in the 600-400 cm^{-1} region, the break down of the DAPS and TPS 20 (and potentially SLO and SVO) sulfide bridges and the formation of any metal-sulfide complexes can be observed. Figure 4.7 shows the far-IR ATR spectra obtained for thermo-oxidatively decomposed DAPS and TPS 20 over the range 100-200 ^{o}C.

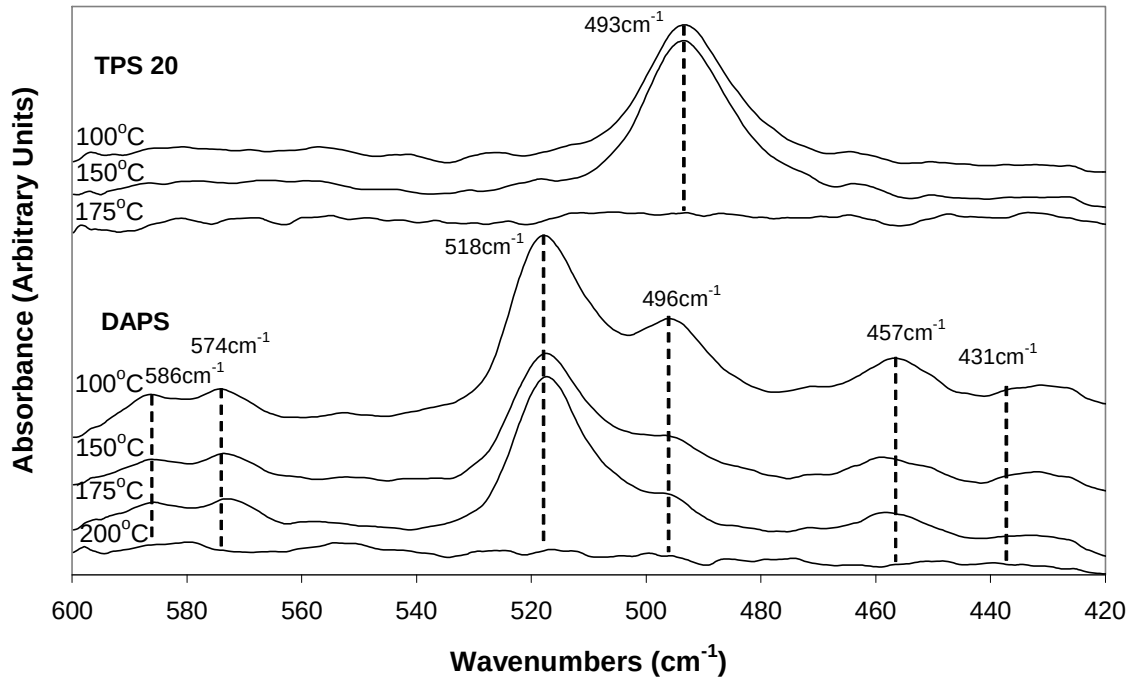

Figure 4.7 Far-IR ATR spectra of thermo-oxidatively decomposed TPS 20 and DAPS in the region 600-420 cm^{-1}.

The thermo-oxidatively decomposed SLO and SVO samples do not exhibit absorptions in the 600-400 cm^{-1} range at any of the temperatures studied (100-500 ^{o}C). This is

consistent with the findings of Najman et al.,[3] who determined that whilst a sulfurised ester thermo-oxidatively decomposed on a steel substrate to form iron sulfate (detectable in the mid-IR at 1200-1185 cm^{-1} and 1415-1380 cm^{-1}),[34] the application of high pressures was required to yield iron sulfides.

The sulfide bridges present in TPS 20 are fully decomposed by ~ 175 ^{o}C; the S-S stretching band at 493 cm^{-1} can no longer be detected. The temperature at which the S-S stretching band disappears corresponds to the onset temperature of mass loss by TGA (172 ^{o}C) and affirms that evaporation dominates the initial stages of the mass loss process. Bands signalling the formation of $[S_2]^-$ and $[S_3]^-$ as a result of S-S bond scission and reaction with the aluminium pan surface are not detectable at 175 ^{o}C.[4, 41] No new absorptions appear in the TPS 20 spectrum at higher temperatures (200-500 ^{o}C) confirming that TPS 20 does not thermo-oxdatively decompose to form detectable amounts of sulfide species.[3, 6]

The thermo-oxidative decomposition process undergone by DAPS is more complex. A decrease in spectral intensity occurs at ~ 150 ^{o}C, corresponding to the onset of mass loss by TGA (150 ^{o}C). The bands at 496 cm^{-1}, 457 cm^{-1} and 431 cm^{-1} broaden and are shifted to higher wavenumber indicating S-S bond decomposition to form alkylthiyl radicals. Similarly, the $[S_2]^-$ and $[S_3]^-$ stretching bands at 586 cm^{-1} and 574 cm^{-1} respectively do not increase in intensity and are shifted to lower wavenumber, suggesting that S-S bond oxidation is taking place. The decrease in spectral intensity and shifts in peak position become more prominent at 175 ^{o}C and by 200 ^{o}C, the six characteristic DAPS absorptions are no longer detectable. This temperature range corresponds roughly to the maximum rate of mass loss temperature (T_{max}) measured for DAPS by TGA (184 ^{o}C) and, as for the other sulfurised additives, verifies that sulfide-type products do not persist until high temperatures under a thermo-oxidative environment.

4.1.3.4 Effect of Sulfur EP Additive Chemical Structure and Concentration on Base Ester Oxidative Stability

The effect of sulfur EP additive chemical structure and concentration on the oxidative

stability of commercial ester A was assessed under continuous heating conditions by measuring the onset temperature of oxidation (PDSC) and mass loss (TGA) of a range of sulfur additive/ester A blends. The results obtained are presented in figure 4.8.

The additives exhibit a neutral effect or increase the oxidative stability of commercial base ester A at all of the sulfur concentration levels studied. This is in accordance with the literature[2, 5, 7, 8, 12, 18] and verifies that the additives possess an anti-oxidant capability. At 0.1 % w/w sulfur concentration, the additives either maintain (SLO and TPS 20) or marginally increase (SVO and DAPS) the ester A PDSC oxidation onset temperature, however all values recorded are within the ± 2 % error margin associated with the measurement. This is in agreement with the findings of Morris and Mushrush,[7] who studied the effects of n-hexyl disulfide and thiophenol on the oxidation of dodecane. The authors found that whilst a mere 0.03 % w/w thiophenol-based sulfur suppressed hydroperoxide formation effectively, the addition of 0.2-0.4 % w/w sulfur in the form of n-hexyl disulfide was required to limit hydroperoxide evolution by 68-46 % respectively. This variation in activity was attributed to differences between the mechanisms via which the two additives inhibit dodecane oxidation, as discussed in Chapter 1. Given that the sulfur-containing additives studied here all possess aliphatic sulfide linkages, their anti-oxidant activity is likely to be similar to that of n-hexyl disulfide such that a more significant amount of additive must be employed before oxidation inhibition is observed.

At 0.5 % w/w sulfur DAPS shows a discernable anti-oxidant effect, increasing the oxidation onset temperature of ester A by 6 ^{o}C to 206 ^{o}C. DAPS displays anti-oxidant activity at lower sulfur concentration than the other three additives, which is related to the ease of oxidation and dissociation of the DAPS pentasulfide bridges and affirms the ATR observations discussed above.[2, 5, 8] DAPS readily forms oxidised sulfur species and alkylthiyl radicals which can respectively reduce or chain-terminate the radicals formed by ester A oxidation to quench hydroperoxide formation.[7, 8, 12, 18]

SLO and SVO begin to exhibit an anti-oxidant effect at 1.0 % w/w sulfur concentration; they increase ester A's oxidation onset temperature to 210 ^{o}C (SLO) and 211 ^{o}C (SVO).

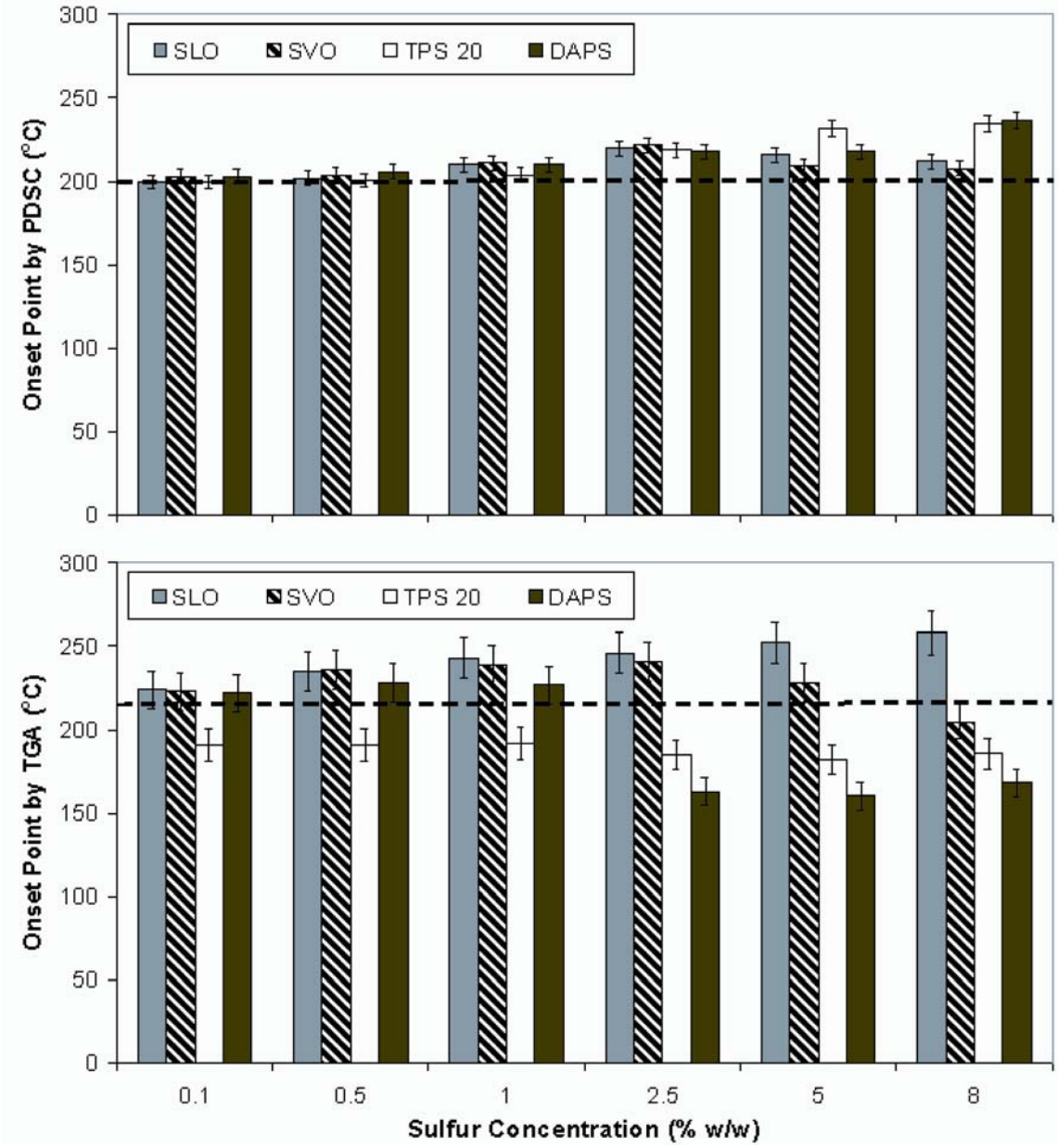

Figure 4.8 Plots of the onset temperature of mass loss (TGA) and oxidation (PDSC) as a function of the % w/w sulfur concentration for blends of SLO, SVO, TPS 20 and DAPS in base ester A. The error bars represent ± 2 % for PDSC and ± 5 % for TGA. The dashed lines indicate the onset temperatures of neat ester A (200 °C by PDSC; 216 °C by TGA).

The higher sulfur concentration required to effect anti-oxidant activity for the SLO and

SVO blends results from the relative stability of the short-chain sulfur bridges contained in these additives and the presence of sulfur in the form of the thermally and oxidatively stable thiophene group.[5, 8, 12] The anti-oxidant activity of DAPS is enhanced at higher sulfur concentration (PDSC T_{onset} = 210 ^{o}C), however it is no greater than that of SLO and SVO. Interestingly, TPS 20 does not improve the oxidative resistance of ester A outside the ± 2 % error margin at 1.0 % w/w sulfur concentration (PDSC T_{onset} = 204 ^{o}C) despite how it contains thermolytically unstable trisulfide bridges.[2, 5] In fact, no anti-oxidant effect for the TPS 20/ester A blends is observed until 2.5 % w/w sulfur concentration. This suggests that either the sulfurised oxidation products formed by TPS 20 react less effectively with radical species produced by ester A oxidation,[12, 18] or that the greater thermal stability of TPS 20 results in the presence of lower concentrations of oxidised sulfur species at the commencement of ester A oxidation.[18] Given that TPS 20 possesses a higher PDSC onset temperature of oxidation than the other three additives (T_{onset} = 220 ^{o}C), that the mid-IR ATR results outlined above indicate a similar oxidised sulfur species profile to DAPS and that the anti-oxidant activity of TPS 20 improves considerably at high dosage levels, the latter of these two explanations in more probable.

The oxidative stability of the DAPS/ester A blends also increases with increasing sulfur concentration and at 8.0 % w/w sulfur, the PDSC oxidation onset temperatures for the TPS 20/ester A and DAPS/ester A blends are 235 ^{o}C and 237 ^{o}C respectively. These values are considerably higher than the onset temperatures of the neat additives (220 ^{o}C for TPS 20 and 182 ^{o}C for DAPS) and suggest that additive-ester interactions promote the oxidative stability of the additives themselves.

The oxidation inhibition activities of SLO and SVO peak at 2.5 % w/w sulfur concentration (PDSC T_{onset} = 220 ^{o}C and 222 ^{o}C for SLO and SVO respectively) and then decrease at 5.0 and 8.0 % w/w sulfur. Although the anti-oxidant effect of sulfur compounds generally improves with increasing sulfur concentration,[18] the decrease in oxidative stability observed for the sulfurised triglyceride blends is consistent with Morris and Mushrush's findings[7] as n-hexyl disulfide was determined to be more effective at inhibiting the evolution of hydroperoxides in dodecane at 0.2 % w/w sulfur

concentration than at 0.4 % w/w. Furthermore, the T_{onset} values at 5.0 % w/w sulfur concentration (216 ^{o}C and 209 ^{o}C for SLO and SVO respectively) approach the T_{onset} values of the neat additives (215 ^{o}C and 209 ^{o}C), inferring that the oxidative stability of the sulfurised triglyceride/ester A blends is dominated by the stability of the additives themselves at high sulfur concentrations.

Further insight into the anti-oxidant behaviour of the four additives is gained by assessing the corresponding TGA mass loss onset temperatures for the additive/ester A blends. At 0.1-1.0 % w/w sulfur concentration, the TPS 20 blends possess an average TGA onset temperature of ~ 191 ^{o}C, 25 ^{o}C below the T_{onset} of neat ester A (216 ^{o}C) and 19 ^{o}C above that of neat TPS 20 (172 ^{o}C). This sulfur concentration regime corresponds to the range over which TPS 20 has very little effect on the oxidative stability of ester A (determined by PDSC) and the mass loss T_{onset} value is ~ 40 ^{o}C below the temperature at which TPS 20 begins to oxidatively decompose (~ 230 ^{o}C, as determined by mid-IR ATR). The TGA onset temperature results obtained therefore represent a combination of the evaporation properties of the two components (191 ^{o}C is close to 194 ^{o}C, the value obtained by averaging the onset temperatures of ester A and neat TPS 20) and confirm that at low sulfur concentrations, TPS 20 is ineffective at suppressing the oxidation of ester A. Although the anti-oxidant activity of TPS 20 improves at higher sulfur concentrations, the TGA T_{onset} values measured over the 2.5-8.0 % w/w sulfur concentration range decrease to an average of 184 ^{o}C. This is due to the dominant effect of TPS 20 on the blends; TPS 20 has a significantly lower onset temperature of mass loss than ester A (172 ^{o}C as opposed to 216 ^{o}C).

The TGA T_{onset} values measured for the DAPS blends follow a similar trend; average mass loss onset temperatures of 228 ^{o}C and 164 ^{o}C are measured over the 0.1-1.0 % and 2.5-8.0 % w/w sulfur concentration ranges respectively (the TGA T_{onset} of neat DAPS is 150 ^{o}C). However in contrast to TPS 20, the successful anti-oxidant activity of DAPS at low sulfur concentrations is manifest in how the average DAPS/ester A blend onset temperature is 12 ^{o}C higher than the T_{onset} of neat ester A alone and is not equivalent to the average of the onset temperatures of the two discrete blend components. This result

once again verifies observations made by PDSC and ATR; DAPS improves the oxidative stability of ester A at lower concentration than any of the other additives as a result of the low temperature at which it decomposes to form sulfurised oxidation products (150-200 ^{o}C, as shown by mid-IR).[18] It should be noted that the high mass loss onset temperature measured for the low sulfur concentration DAPS blends is tempered by the volatility of DAPS and its sulfurised oxidation products. Consequently, the drop in T_{onset} observed at higher sulfur concentrations is due to the dominant effect of DAPS on the blends.

At 0.1 % w/w sulfur concentration, the TGA onset temperatures for the SLO and SVO blends are 224 ^{o}C and 223 ^{o}C respectively. As for the DAPS blends, these values are greater than the T_{onset} values of the neat additives (158 ^{o}C for SLO and 168 ^{o}C for SVO) and neat ester A (216 ^{o}C) and verify the formation of sulfurised oxidation products at lower temperatures. However, unlike DAPS, the sulfurised triglyceride blend mass loss onset temperatures increase with increasing the sulfur concentration. For SLO, this increase is observed over all concentration levels such that at 8.0 % w/w sulfur, the onset temperature of mass loss is 258 ^{o}C, 42 ^{o}C greater than the T_{onset} of ester A and 100 ^{o}C greater than that of neat SLO. In contrast, the SVO blends only show an increase in T_{onset} until a sulfur concentration of 2.5 % w/w is reached (T_{onset} = 241 ^{o}C); at 5.0 % w/w sulfur, the T_{onset} value drops to 228 ^{o}C and continues to decrease at higher sulfur concentration levels. This is related to the decomposition of SVO to form a significantly greater proportion of volatiles than SLO at low temperatures; at 215 ^{o}C, approximately 28 % of SVO sample mass has been lost in comparison to only 10 % for SLO (refer to figure 4.1 and table 4.2). The high level of mass loss that occurs in SVO ~ 200 ^{o}C mitigates any increase SVO affects on the TGA mass loss onset temperature of ester A, particularly at high sulfur concentrations.

4.1.3.5 Effect of Sulfur EP Additive Chemical Structure and Concentration on Base Ester Residue Levels

The effect of sulfur EP additive chemical structure and concentration on the residue-

forming tendency of commercial base ester A can be determined by calculating the % B/A ratio from TGA and PDSC data according to equation 3.1.[27, 28] The temperature ranges over which the primary (A) and secondary (B) decomposition regions are defined are the same as for the triglycerides and commercial base esters studied in Chapter 3.2; mass loss and heat flow events in the range 300-500 ^{o}C are included within 'B' and those occurring between room temperature and 300 ^{o}C are included within 'A'. Figure 4.9 shows an overlay of the DTG curves obtained for blends of SLO, SVO, TPS 20 and DAPS at 1.0 % w/w sulfur concentration in ester A.

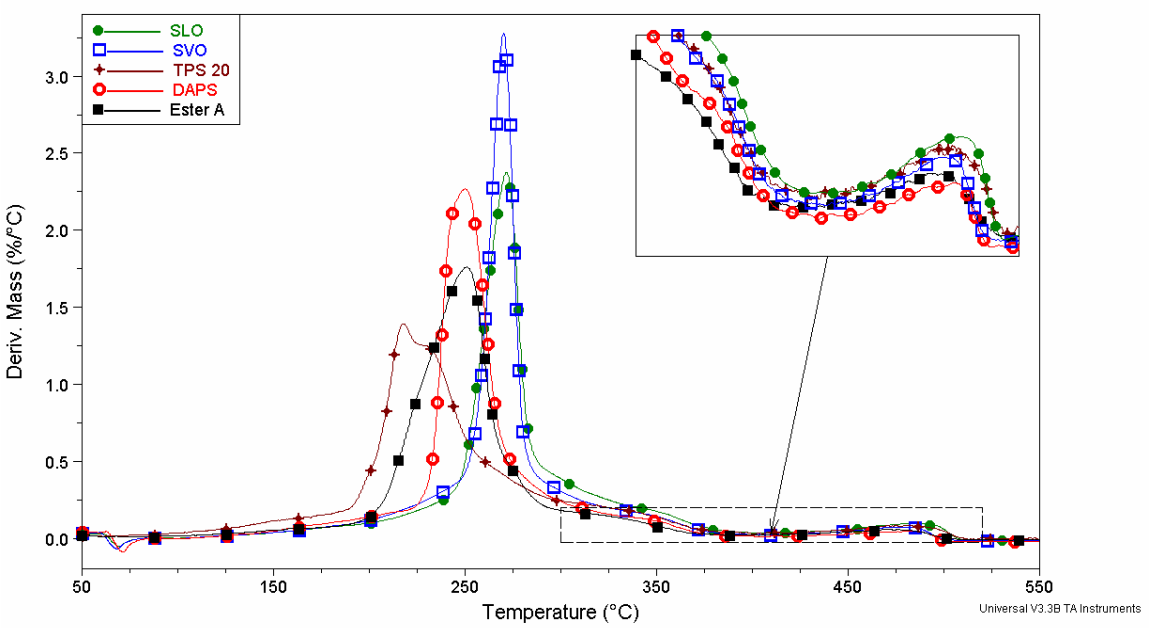

Figure 4.9 Overlay of the TGA thermo-oxidative decomposition profiles (DTG curves) of SLO, SVO, TPS 20 and DAPS blends at 1.0 % w/w sulfur concentration in base ester A. The inset view highlights the secondary decomposition region (300 ^{o}C-500 ^{o}C).

It is evident that thermo-oxidative mass loss events occur in the range 300-500 ^{o}C (the secondary, or B, decomposition region) for all four additive/ester A blends. An analogous observation is made by PDSC and secondary region mass loss (TGA) and heat flow (PDSC) events are detected at all of the sulfur additive concentrations levels

studied. This can be contrasted with the TGA and PDSC results obtained for the neat sulfurised additives. Only neat SLO and SVO undergo mass loss at temperatures above 300 ^{o}C by TGA; the TGA thermo-oxidative decomposition profiles of neat DAPS and TPS 20 show that essentially all sample mass is lost below 300 ^{o}C.

Similarly, although the four sulfurised additives display heat flow events over the PDSC secondary decomposition region, the enthalpy associated with these events for DAPS and TPS 20 is negligible in comparison to that measured for SLO and SVO (refer to table 4.2). Thus, the presence of mass loss (TGA) and heat flow (PDSC) events over the secondary decomposition region for the DAPS and TPS 20 blends results from the thermo-oxidative decomposition reactions of ester A. The impact of each of the sulfurised additives on the proportion of mass loss and heat flow undergone by ester A over the secondary decomposition region is shown in figure 4.10 as a plot of the PDSC and TGA % B/A ratios as a function of the % w/w sulfur concentration.

All four additives increase the ester A PDSC % B/A ratio at 0.1 % w/w sulfur concentration. The level of increase is greater for the sulfurised triglycerides (particularly SVO, which gives a % B/A ratio value of 6.5 %, more than four times that of neat ester A) than for DAPS and TPS 20. Given that the enthalpy of reactions occurring within the secondary decomposition region is associated with combustion and/or thermal cracking of high molecular weight and crosslinked material,[27, 28] the increase in the % B/A ratio suggests that addition of the sulfurised additives at low sulfur concentrations promotes the formation of residues that decompose to release proportionately more energy than residues formed by ester A alone.[7]

Comparison between the PDSC % B/A ratios at 0.1 % w/w sulfur concentration with those determined by TGA reveals that the additives increase the energy released by residue decomposition as opposed to the amount of residue formed (although SLO and SVO do increase the TGA % B/A ratio marginally). Since the branched and/or crosslinked material decomposed over the secondary decomposition region is formed by the reactions of sulfur, oxygenated and alkyl radical species with C=C bonds,[7, 21, 25, 26] the % B/A ratio results imply that the incorporation of sulfur into the residue structure

increases the enthalpy of combustion/decomposition of this material.

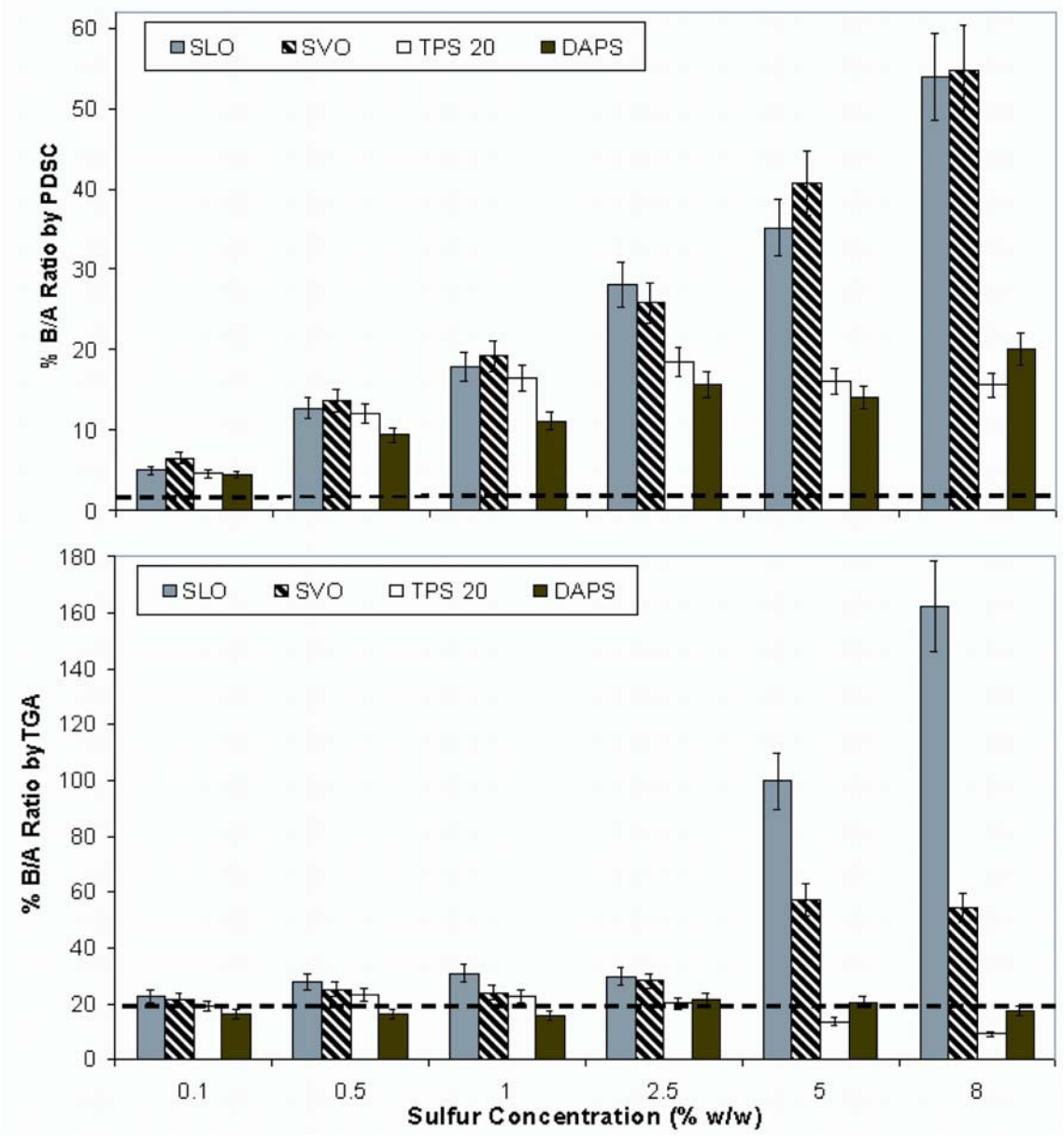

Figure 4.10 Plots of the TGA and PDSC % B/A ratios as a function of the % w/w sulfur concentration for blends of SLO, SVO, TPS 20 and DAPS in base ester A. The error bars represent ± 10 % error. The dashed lines indicate the ester A % B/A ratio (1.6 % by PDSC; 18 % by TGA).

This is consistent with the greater enthalpies associated with the combustion of simple

sulfur-containing hydrocarbons as opposed to simple hydrocarbons; $\Delta H_c^{o}{}_{ethane(g)}$ = -373 kcal mol^{-1}, $\Delta H_c^{o}{}_{ethanethiol(l)}$ = -519 kcal mol^{-1}; $\Delta H_c^{o}{}_{propane(g)}$ = -531 kcal mol^{-1}, $\Delta H_c^{o}{}_{1\text{-}propanethiol(l)}$ = -676 kcal mol^{-1}.[44]

The higher PDSC % B/A ratios determined for the sulfurised triglyceride blends are due to C=C bonds present in both the additives and in the products formed by their thermal decomposition elevating unsaturation levels and thereby increasing the amount of branched and/or crosslinked residues formed. SVO affects the greatest increase in ester A's % B/A ratio as it contains the shortest average S-S chain length and decomposes to form a greater number of alkylthiyl radicals than SLO. The branched and/or crosslinked residues formed by the SVO blend therefore contain a higher proportion of sulfur and evolve more energy during combustion and thermal decomposition.[44]

As the level of sulfur contained in the additive blends is raised, the increase in the PDSC % B/A ratio becomes more pronounced, particularly for the sulfurised triglycerides. At 8.0 % w/w sulfur concentration, the PDSC % B/A ratios for the SLO and SVO blends are 54 % and 55 % respectively, more than thirty times greater than the % B/A ratio of neat ester A. For the DAPS and TPS 20 blends, the PDSC % B/A ratio increases until ~ 2.5 % w/w sulfur concentration and then remains relatively constant at higher sulfur levels; the average % B/A ratio for both additives in the 2.5-8.0 % w/w sulfur concentration range is 17 %, ten times greater than the % B/A ratio of neat ester A. This observation implies that the residues formed by the DAPS and TPS 20 blends are of similar chemical structure at sulfur concentration levels of 2.5 % w/w or more and that the energy evolved by the thermo-oxidative decomposition of these residues does not vary considerably. Since the formation of high molecular weight branched and/or crosslinked material in the DAPS and TPS 20 blends is dependent on the presence of C=C bonds in the ester A alkyl chains (the additives themselves contain saturated hydrocarbon chains), it is likely that above a certain sulfur concentration level sulfur branches and/or crosslinks can no longer be incorporated into the residue structure (ie the residue reaches a 'sulfur saturation level'). At higher sulfur concentrations, excess alkylthiyl radicals and any alkyl radicals formed by C-S bond scission eventually

decompose and therefore do not contribute substantially to the formation of thermally stable deposits.[18] This is in agreement with the TGA % B/A ratio results for the DAPS and TPS 20 blends. At all of the sulfur concentration levels studied, DAPS and TPS 20 do not increase the amount of thermally-stable residue formed outside of the ± 10 % error margin. On the contrary, at high sulfur concentrations the additives lower the % B/A ratio and promote volatilisation over the primary decomposition region. This is consistent with the findings reported by Sech and Oleksiak,[13] who established that sulfurised hydrocarbon additives reduce the amount of residue formed by rolling oil decomposition under a 6 % H_2-94 % N_2 batch annealing atmosphere. Sech and Oleksiak proposed that interactions between the 'active' sulfur and the metal surface preclude the adhesion of ester groups and the formation of soap-like residues. However, they also found that sulfurised fat reduces the level of residue formed by rolling oil decomposition. This is contrary to the results in the present study; SLO and SVO both increase the TGA % B/A ratio, particularly at sulfur concentrations above 2.5 % w/w. In addition, the mid-IR ATR results discussed above clearly show that soap-like residues are formed during the sulfurised triglyceride thermo-oxidative decomposition process. Therefore, in accordance with the SLO and SVO thermo-reductive decomposition results presented above, the reduction in residue levels attained by Sech and Oleksiak through the incorporation of sulfurised fat into a rolling oil formulation appears to flow from the use of an HNX atmosphere.

4.1.3.6 Residue Impact on 55Al-43.4Zn-1.Si Coating Quality

Links between 55Al-43.4Zn-1.6Si coating quality and the chemical nature of both the sulfurised additives and their thermal decomposition residues have been assessed by performing hot dip metallic coating simulations. Figure 4.11 shows optical microscopy images of 55Al-43.4Zn-1.6Si coated samples created using steel treated with neat SLO, SVO, TPS 20 and DAPS.

All four sulfurised additives impact detrimentally on 55Al-43.4Zn-1.6Si coating quality in comparison to the steel control sample. Two classes of uncoated defects, base-

uncoated and intermetallic-uncoated, are present in the DAPS and TPS 20 samples, whilst only base-uncoated defects are evident for the sulfurised triglyceride samples.

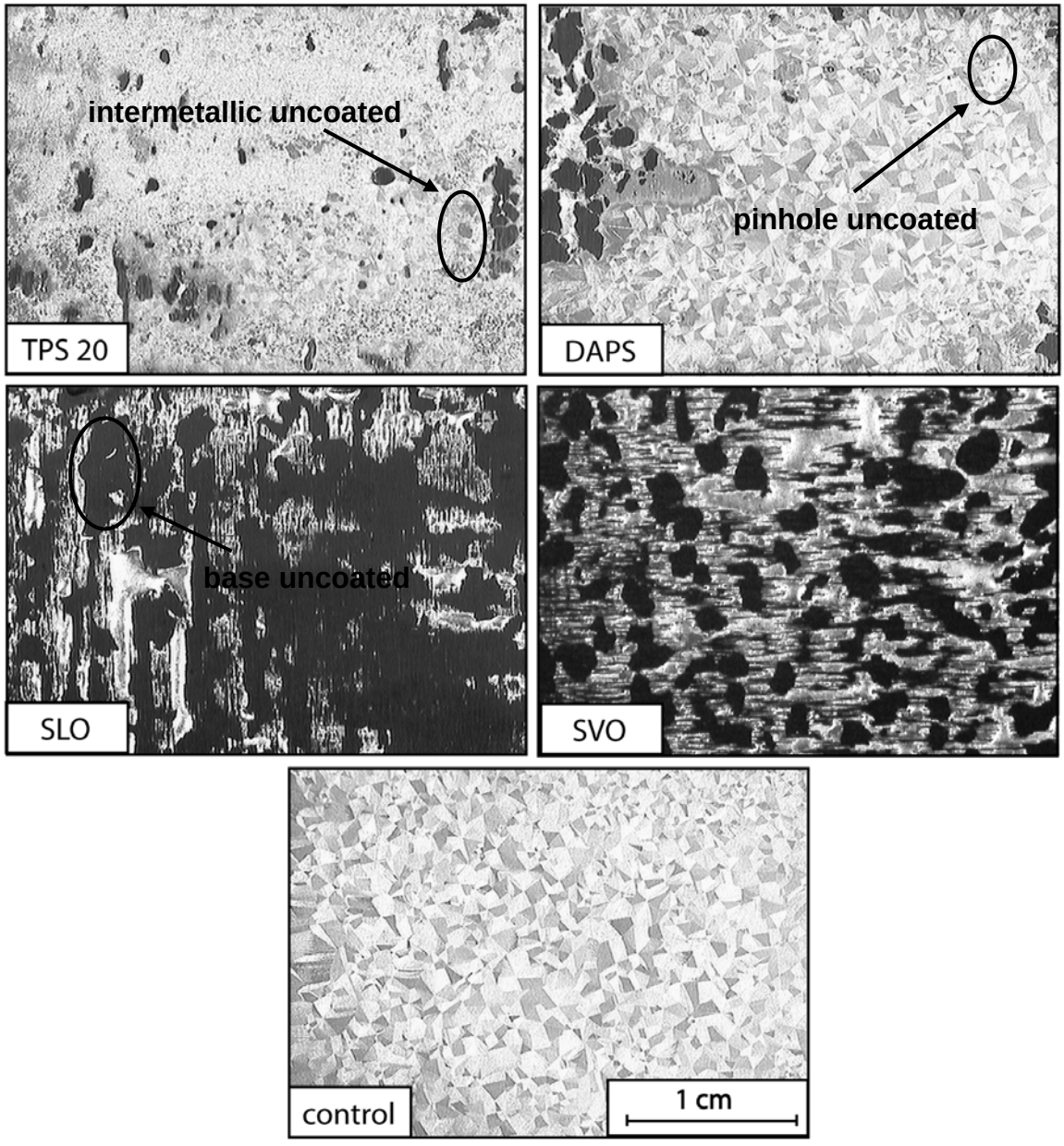

Figure 4.11 Optical microscopy images of 55Al-43.4Zn-1.6Si coated steel samples prepared using the hot dipping simulator after the application of neat TPS 20, DAPS, SLO or SVO. A control sample prepared from untreated steel is shown for comparison.

The base-uncoated defects (described in Chapter 3.2) appear as dark regions in the figure 4.11 images. The detection of these areas suggests that the residues formed by the additive decomposition process impede the wettability of the steel surface by the molten alloy. [10, 11, 45] The intermetallic-uncoated defects observed for the DAPS and TPS 20 samples are characterised by regions where the alloy overlayer is absent and the intermetallic layer is exposed. The TPS 20 sample in particular displays intermetallic-uncoated defects which appear as grey regions where no light-coloured alloy overlayer is present. As for the base-uncoated defects described above, intermetallic-uncoated defects can be attributed to lower reactivity between the steel substrate and the molten Al-Zn alloy and are also likely to result from the presence of steel surface contaminants.[46] Although the majority of uncoated defects present in the samples are gross in nature (refer to discussion in Chapter 3.2), the DAPS and TPS 20 samples also display medium, fine and pinhole uncoated regions. The smaller-scale uncoated defects are likely to result from bridging effects, whereby the alloy overlayer solidifies over the top of the uncoated steel substrate.[45]

The DAPS-treated sample displays the best coating quality; approximately 93 % of the steel surface is covered by the metallic coating (the steel control sample exhibits 99 % coating coverage) and well-formed spangles are clearly visible in the alloy overlayer. Although steel surface treatment with TPS 20 only results in a slightly poorer metallic coating coverage (92 %), no spangles are present in the coating overlayer. This could be an artefact of the hot dip simulation process or it could suggest that the products formed by TPS 20 decomposition interfere with the normal spangle nucleation and growth mechanism.[46]

The sulfurised triglycerides have a more severe impact upon metallic coating quality. The metallic coating on the SVO-treated sample is barely adhered to the steel substrate and only 34 % surface coverage is achieved. Some alloy overlayer has solidified on the surface giving the sample a network-like appearance, however no spangles are present. The results obtained for the SLO-treated sample are similar and SLO produces the worst coating of the four sulfurised additives; only 28 % of the steel sample surface is covered.

These results confirm that the thermally-stable deposits formed by the thermo-reductive decomposition of the sulfurised additives interfere with metallic coating quality. The deposits formed by the sulfurised triglycerides, which consist primarily of organo-carboxylates, non-volatile radical recombination products and aromatic species, impact more severely upon coating quality than do the deposits formed by the sulfurised hydrocarbons. Given that additional residues are formed in the presence of oxygen (non-volatile sulfur oxidation products and oxygenated radical recombination products), the impact of sulfurised additive thermo-oxidative decomposition deposits on metallic coating quality is likely to be more severe.

Figure 4.12 shows images of 55Al-43.4Zn-1.6Si coatings prepared from blends of TPS 20 and SLO in commercial base ester A in the 0.1-8.0 % sulfur concentration range. The results presented are representative of those obtained for the DAPS and SVO blends.

The TPS 20 blend samples show normal spangle characteristics, confirming that that lack of spangles observed for the neat TSP 20 sample is an artefact of the hot dip simulation process. TPS 20 has very little impact upon metallic coating quality up until ~ 2.5 % w/w sulfur concentration and at low sulfur concentrations, the coating quality appears to be superior to that of the neat ester A sample. This is in agreement with the findings of Sech and Oleksiak[13] and with the % B/A ratio results presented above; TPS 20 does not dramatically increase either the amount of residue formed by the decomposition of ester A or the chemical structure of this residue. At higher sulfur concentrations, TPS 20 does induce the formation of gross and pinhole base-uncoated defects suggesting that despite the ATR results presented above, it decomposes to form residues which affect the wettability of the steel surface by the alloy coating.

As for TPS 20, SLO has no discernable effect on metallic coating quality at 0.1 % w/w sulfur concentration; the spangles formed are of similar appearance to the control sample and there is no increase in uncoated defect levels. However, at 0.5 % w/w sulfur concentration, pinhole and fine uncoated defects appear in the coating. These defects worsen at 1.0 % w/w sulfur concentration; medium to gross base-uncoated defects and intermetallic-uncoated defects are apparent.

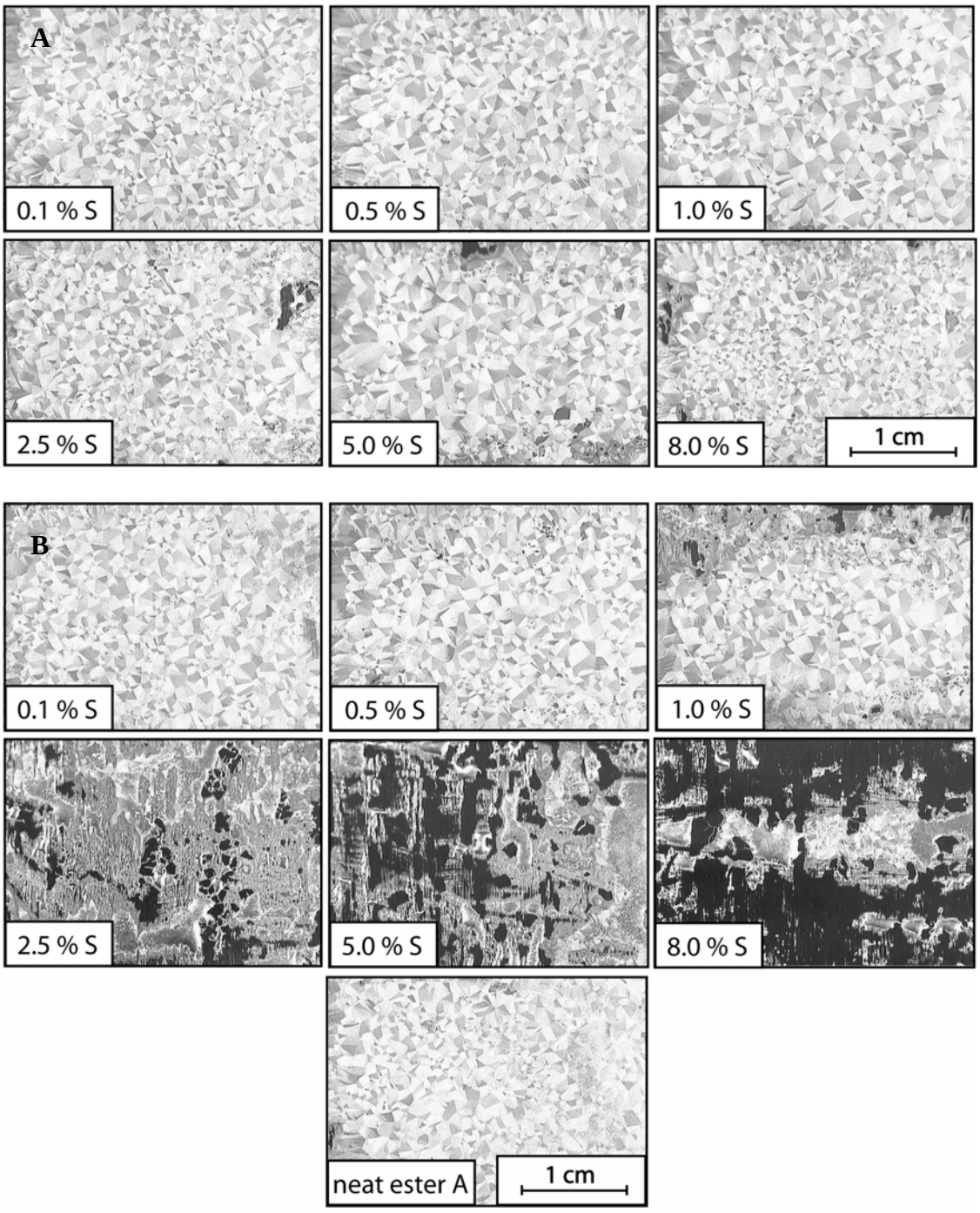

Figure 4.12 Optical microscopy images of 55Al-43.4Zn-1.6Si coated steel samples prepared using the hot dipping simulator after the application of blends of TPS 20 (A) and SLO (B) at different sulfur concentrations in base ester A. A control sample prepared from steel treated with neat ester A is shown for comparison.

The detrimental impact of SLO on metallic coating quality is consistent with the higher residue levels detected by TGA at 500 ^{o}C for SLO under both thermo-oxidative (11 %) and thermo–reductive (3.4 %) conditions, and with % B/A ratio results presented above; at 0.5 % w/w sulfur concentration, the addition of SLO to ester A increases the amount of thermally stable residue formed. These results affirm that the carboxylate, non-volatile radical recombination and aromatic residues formed by SLO decomposition impact more detrimentally upon steel surface wettability than do the residues formed by decomposition of the sulfurised hydrocarbons. This could be due to greater carbonaceous (hydrophobic) nature of the sulfurised triglyceride residue.[11]

The spangles formed in the SLO blend coatings are of normal appearance up until 2.5 % w/w sulfur concentration, when a large proportion of the sample surface contains gross base-uncoated and intermetallic-uncoated defects. The network-like structure of the coating results from poor surface wettability.[45] The metallic coating quality continues to degrade at higher sulfur concentration levels and at 8.0 % w/w sulfur, the majority of steel surface is uncoated. These observations once again support the % B/A ratio results presented above; at high sulfur concentrations SLO causes the formation of significantly more residue that is of different chemical structure to that formed by the decomposition of ester A alone. The impact of sulfur additive chemical structure and concentration on metallic coating quality is further illustrated in figure 4.13.

Despite the significant error margins associated with quantifying the % uncoated defect area, the graph presented in figure 4.13 shows a definitive trend towards increasing levels of uncoated defects with increasing sulfur concentration, particularly for the sulfurised triglycerides. At 0.1 % w/w sulfur concentration, neither the sulfurised triglycerides nor the sulfurised hydrocarbons increase the uncoated defect area above that of neat ester A. However at 1.0 % w/w sulfur concentration, SVO and SLO cause the level of uncoated defects to increase by 3.5 % and 2.9 % respectively, a trend propagates exponentially with increasing sulfur concentration. SLO causes more uncoated defects in comparison to SVO at similar sulfur concentration, an observation which is in agreement with % residue levels measured at 500 ^{o}C for the two additives

(11 % and 6.8 % for SLO and SVO respectively under HNX) and with TGA % B /A ratio results. In contrast, the sulfurised hydrocarbons improve metallic coating quality at concentrations below 2.5 % w/w sulfur. At higher sulfur concentrations, TPS 20 increases the uncoated defect area marginally whilst DAPS has no discernable impact unless it is applied neat.

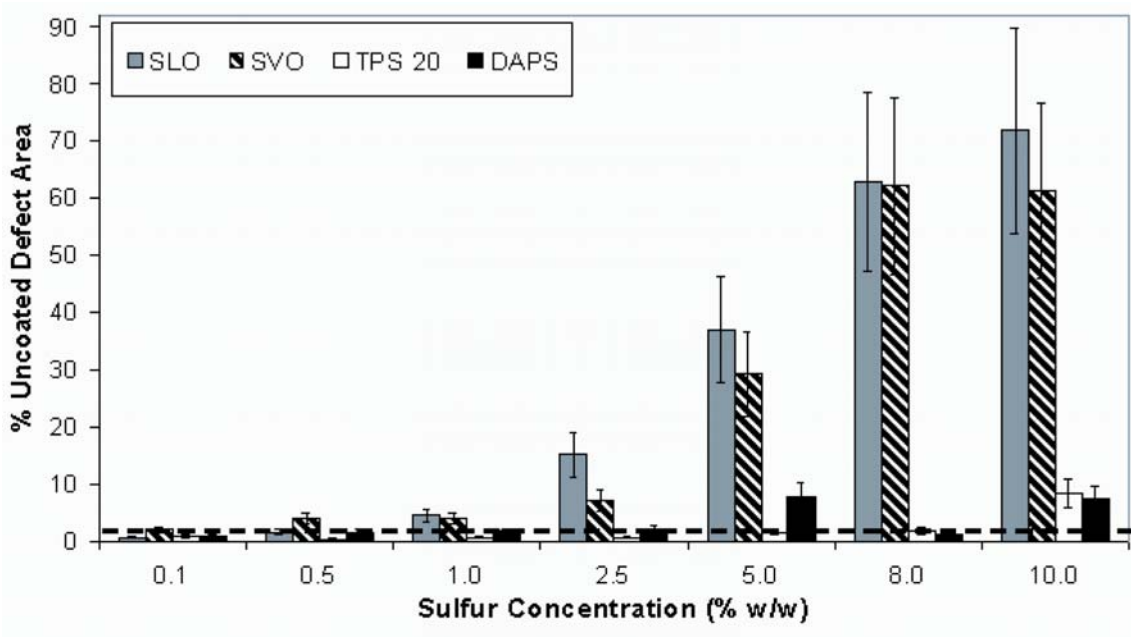

Figure 4.13 Plot of the % uncoated defect area as a function of % w/w sulfur concentration for 55Al-43.4Zn-1.6Si coated samples prepared from steel treated with blends of SLO, SVO, TPS 20 and DAPS in base ester A. The error bars represent ± 25 % error. The dashed line indicates the % uncoated defect area determined for a neat ester A sample (% uncoated defect area = 1.2 %).

These results confirm that the residues formed by thermal decomposition of SLO and SVO cause the formation of uncoated defects in 55Al-43.4Zn-1.6Si and suggest that sulfurised hydrocarbons can potentially be incorporated into cold rolling oil formulations at relatively high concentrations (> 2.5 % w/w sulfur) without impacting detrimentally upon metallic coating quality.

4.1.3.7 ToF-SIMS Characterisation of Uncoated Defects

ToF-SIMS analysis of a steel control together with neat DAPS- and SLO-treated hot dip simulation samples was performed to elucidate the chemical nature of steel surface residues giving rise to uncoated defects. Figure 4.14 shows a negative ion spectrum obtained within an uncoated defect present in a DAPS-treated sample.

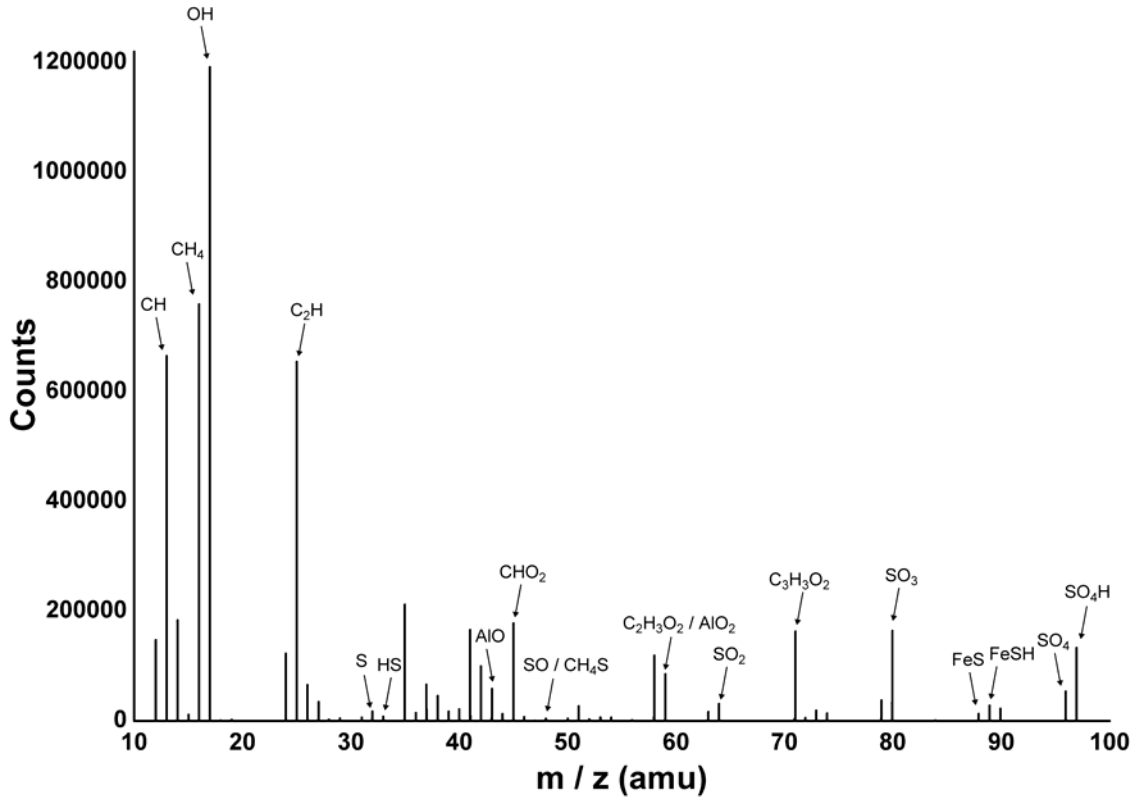

Figure 4.14 ToF-SIMS negative ion spectrum obtained in an uncoated area present in a neat DAPS-treated hot dip simulation sample.

Numerous peaks relating to steel substrate oxides (FeO, FeOH), oxides of the alloy coating material (Al, AlO), sulfides, sulfur oxides and sulfur-containing hydrocarbons (^{32}S, SO_x, FeS, FeSH), hydrocarbons and oxidised hydrocarbons (CH_y, $C_xH_yO_z$) and high molecular weight hydrocarbons and oxidised hydrocarbons (data not shown; m/z > 250 amu) are evident. The relatively low ion counts measured for the sulfur-containing

species is consistent with the ATR results above and confirms that the concentration of residual sulfides and sulfur oxides is below the infrared spectrophotometer detection limit. Similar peaks are present in spectra acquired within uncoated defect areas in the SLO-treated sample, however elemental sulfur, iron sulfides, sulfur oxides and carbonaceous sulfur species are also evident in the untreated steel control sample spectra. This implies that sulfur derived from both the steel substrate (~ 0.014 % w/w sulfur) and the sulfurised EP additives contributes to the sulfur-based species detected. In order to distinguish between the sulfur-containing peaks present in the control sample spectrum and the two additive-treated sample spectra, depth profiles monitoring eight sulfur-containing ions were acquired (figure 4.15).

The depth profile shown for the steel control sample reveals that the normalised intensities of the sulfur ions, determined according to equation 2.4 in Chapter 2, remain relatively constant as the number of sputtering cycles (depth into the sample surface) increases. In addition, the normalised ion intensities are much lower for the steel control than for the two additive-treated samples. These observations suggest that the sulfur species detected on the steel control sample are derived from sulfur contained within the steel substrate.In contrast, the DAPS-treated sample depth profile displays normalised ion intensities that are up to five times greater than for the steel control. An initial peak in the normalised intensity of all ions except SO_3 and SO_4 is observed, followed by a gradual decay in intensity as the number of sputtering cycles (depth) increases. These observations, together with the eventual plateau in the ion intensities at a level similar to that observed for the steel control, confirm that a sulfur-containing residue layer formed by decomposition of the DAPS additive is present on the steel surface.

In contrast to the far infrared ATR results, the composition of this residue layer is dominated by sulfide species, as indicated by the greater normalised intensity of the ^{32}S and FeS ions. This and the comparatively low intensity of sufur oxide species (SO, SO_2, SO_3, SO_4) is due to the preparation of the hot dip simulation samples under an HNX atmosphere; in presence of oxygen, these species are likely to be more abundant. CH_4S is also relatively abundant, implying the presence of sulfur-containing hydrocarbons.

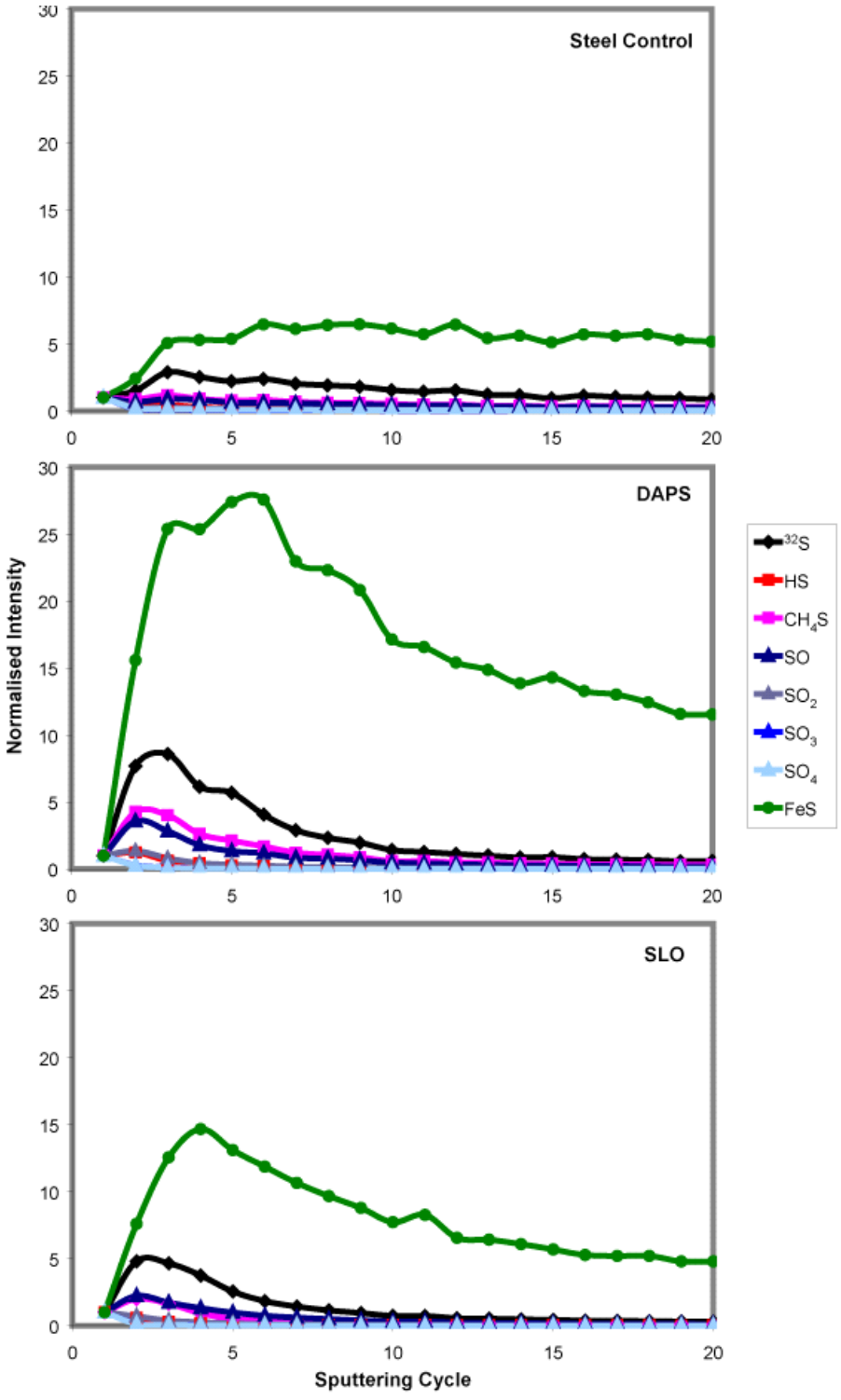

Figure 4.15 Normalised depth profiles obtained for a steel control and neat DAPS- and SLO-treated samples.

The SLO-treated sample displays a similar depth profile to that observed for the DAPS-treated sample, verifying that sulfur-containing residues are formed by decomposition of the SLO additive. Furthermore, the normalised intensities of all the sulfur-containing ions is lower for the SLO-treated sample than for the DAPS-treated sample. This is consistent with observations made by ATR that the composition of the SLO residue is dominated by carboxylate species and radical recombination products.

4.1.4 Conclusions

The thermo-oxidative and -reductive decomposition properties of four sulfurised EP lubrication additives and their blends in a commercial cold rolling base ester have been studied by TGA and PDSC. The results reveal that sulfur EP additive chemical structure has a significant impact upon residue levels, with sulfurised triglycerides leaving up to six times more residue at 500 ^{o}C than sulfurised hydrocarbons. However, the branching and/or crosslinking reactions that give rise to these high residues levels are suppressed under an HNX atmosphere, lowering the level of residue formed by the sulfurised triglycerides by more than 50 %.

The chemical nature of this residue, analysed by mid- and far-infrared spectroscopy, is highly dependent upon the additive structure. The sulfurised triglycerides decompose to form carboxylate complexes, non-volatile radical recombination products and aromatic species, however the residues formed by the sulfurised hydrocarbons are below detection limits.

The results of experimental hot dipping simulations show that although both sulfurised triglyceride and sulfurised hydrocarbon EP additives give rise to 55Al-43.4Zn-1.6Si uncoated defects, the detrimental impact of the sulfurised triglycerides is far more severe. ToF-SIMS analysis of the steel surface chemistry within uncoated defect areas suggests that this is due to the hydrophobic nature of the sulfurised triglyceride residue; the predominantly carboxylate- and radical recombination product-based residues formed by sulfurised triglycerides have a greater detrimental impact upon metallic coating quality than do the sulfur-based residues formed by sulfurised hydrocarbons.

Given these results, the potential exists for minimising the formation of harmful steel surface residues through the use of thermo-reductive as opposed to thermo-oxidative conditions. In addition, use of sulfurised hydrocarbons as EP lubrication additives provides grater scope for tailoring sulfur additive concentration to enhance lubrication performance and oil oxidative stability without impacting detrimentally upon metallic coating quality.

4.2 Impact of Phosphate Anti-Wear Additive Thermal Decomposition Products on 55Al-43.4Zn-1.6Si Coating Quality

4.2.1 Introduction

Alkyl phosphates are an ideal class of compounds for use in a variety of industrial high temperature applications as a result of their superior resistance to thermal and oxidative degradation. They are commonly employed as fire-retardants in cellulose-based fabrics[47, 48] and other polymeric materials[49-51] and they are often substituted for hydrocarbon-based lubricant fluids in mechanical systems exposed to extreme high temperature conditions.[49, 51-54] Furthermore, incorporation of alkyl phosphates into metal-working fluids offers two-fold benefits; the surfactant characteristics of alkyl phosphates aid in lubricant emulsification and the affinity of the phosphate head group for metal surfaces gives rise to the excellent anti-wear (AW) properties of these compounds.[6, 49, 51, 53-60]

Two of the most common types of alkyl phosphate additives used in metal forming lubricants are phosphate esters and amine phosphates.[56] The generic chemical structures of these two classes of compounds are shown in scheme 4.2. Phosphate esters decompose upon the application of high temperatures and/or pressures to form a tribofilm that has been described in the literature as comprising of metal polyphosphates, metal phosphates/phosphides and metallic/organic phosphates.[6, 57-63] Amine phosphates generate metal polyphosphates in an extreme-pressure (EP) environment,[58] although

they may decompose to form ammonium-containing compounds under boundary lubrication conditions.[6, 62]

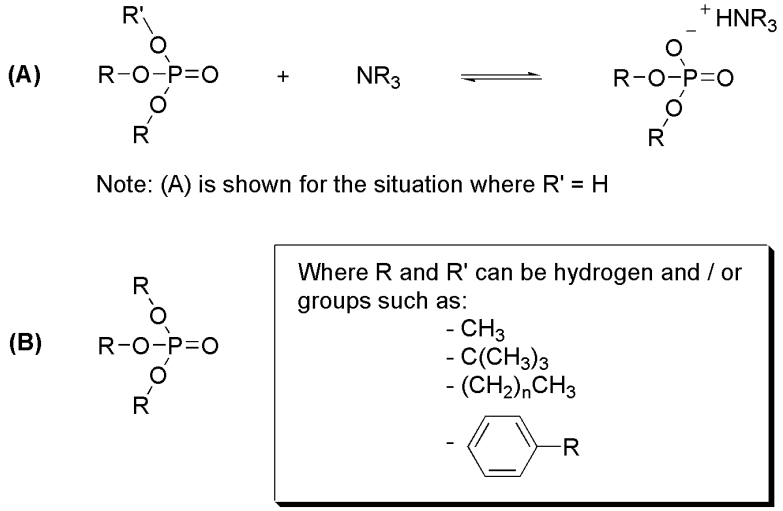

Scheme 4.2 Structural representation of a typical amine phosphate (A) and phosphate ester (B).

Although phosphorus additives are typically employed in commercial cold rolling oil formulations to perform an anti-wear function, they have been shown to improve lubricity in a similar manner to sulphur EP additives.[56] Thus, subject to the lubrication requirements of individual cold rolling mills, the possibility exists for optimising phosphorus additive concentration to improve both lubrication and anti-wear properties. However, phosphorus additives are highly surface-active compounds and they have been shown to compete other ingredients (such as base oils and sulphur EP additives) for adsorption to metal surfaces.[58, 61] Hence, the deposit-forming tendencies of phosphorus AW additives are of considerable interest in the metallic coatings industry; the formation of persistent steel surface residues following the cold rolling and furnace cleaning processes may impact detrimentally upon metallic coating quality. [10, 11, 46, 64]

The thermal and oxidative degradation of neat phosphate AW additives and their blends in a range of base oils has been studied extensively using both thermal analysis and spectroscopic techniques.[6, 49, 51-54, 56-61, 63, 65, 66] The formation of significant amounts of

'char-like' residue has been noted.[50, 52] However, the majority of studies have focussed on the lubrication properties of phosphate AW additives and their thermal decomposition products; the impact of phosphate AW additive residues upon metallic coating quality has never been investigated.

This work uses TGA and PDSC techniques to study the thermo-oxidative decomposition and residue formation properties of two phosphate-based AW additives commonly used in commercial cold rolling formulations; a tri-alkyl phosphate ester and an aromatic amine phosphate. The chemical composition of the thermo-oxidative decomposition residues formed by these additives is characterised by ATR and the residue impact on 55Al-43.4Zn-1.6Si hot dip metallic coating quality is evaluated through the performance of simulated hot dipping trials.

4.2.2 Experimental

4.2.2.1 Sample Preparation

4.2.2.1.1 Materials

The phosphate ester and amine phosphate additives used in this section were supplied by Quaker Chemical (Australasia). The chemical structures of these additives are proprietary, however general structural representations are given in scheme 4.2. Table 4.8 summarises the total concentration of sulfur (% w/w) contained in each additive and figure 4.16 shows the mid-infrared ATR spectra obtained for the neat additives. Of interest is the O-H stretching absorption present in both spectra at 3378-3368 cm^{-1} which is indicative of free hydroxyl moieties on the phosphate head group.

Table 4.8 Total concentration of phosphorus in each of the phosphorus additives.

Additive	Phosphorus Concentration (% w/w)
phosphate ester	5.8
amine phosphate	4.7

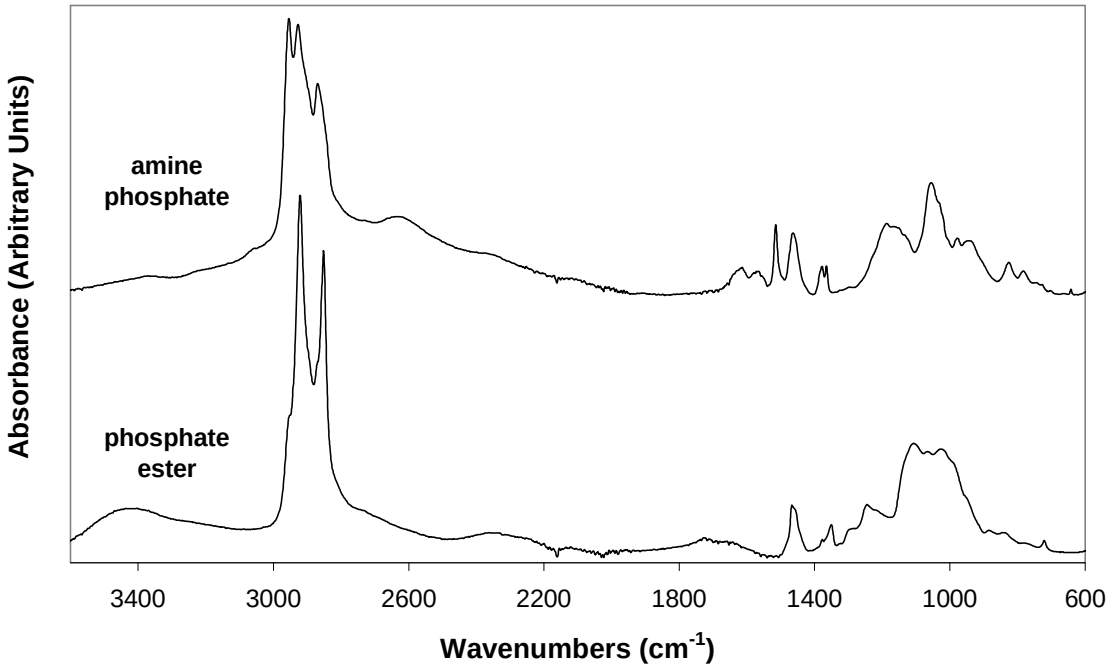

Figure 4.16 Mid-IR ATR spectra of the neat amine phosphate and phosphate ester additives.

The chemical characteristics of ester A, a typical commercial cold rolling oil base ester, are described in Chapter 3 (refer to section 3.2.2.1.1).

The properties of the other materials used are described in Chapter 2.2 as follows:

- cold rolled steel - table 2.3;
- 55Al-43.4Zn-1.6Si alloy - table 2.4;
- shellite and ethanol solvents - section 2.2.5;
- oxygen and HNX gases - section 2.2.6, and
- TGA and PDSC consumables - section 2.2.7.

4.2.2.1.2 Phosphorus Additive/Ester A Blends

Blends of each of the phosphorus additives in commercial base ester A at 0.05, 0.1, 0.5, 1.0 and 2.5 % w/w phosphorus concentration were prepared according to the method described in Chapter 2 (refer to section 2.3.1.2).

4.2.2.1.3 Sample Preparation for ATR

The neat phosphorus additives were prepared for mid-infrared ATR analysis according to the procedure described in Chapter 2 (refer to section 2.3.2). The process of phosphorus additive thermo-oxidative decomposition is well-known such that the chemical structure of the residue remaining after (as opposed to the chemical changes occurring during) the thermo-oxidative decomposition process was of particular interest. Thermo-oxidatively decomposed phosphorus additive samples were therefore prepared at a single temperature: 500 ^{o}C.

4.2.2.1.4 Preparation of Hot Dip Simulation Samples

55Al-43.4Zn-1.6Si hot dip metal-coated samples were prepared using neat phosphorus additives and their 2.5 % w/w phosphorus blends in commercial base ester A (representing the 'worst case scenario') according to the hot dip simulation procedure described in Chapter 2 (refer to section 2.3.3).

4.2.2.2 Characterisation Techniques

4.2.2.2.1 TGA

The thermo-reductive decomposition profiles of the neat phosphorus additives and the thermo-oxidative decomposition profiles of the neat phosphorus additives and their 0.05 and 2.5 % w/w phosphorus blends in ester A were analysed by TGA under HNX and oxygen respectively according to the conditions and procedure described in Chapter 2 (refer to section 2.4.1).

4.2.2.2.2 PDSC

PDSC analysis of the neat phosphorus additives and their 0.05 and 2.5 % w/w phosphorus blends in ester A was performed according to the procedure described in Chapter 2 (refer to section 2.4.2).

4.2.2.2.3 ATR

The parameters used to collect mid-infrared ATR spectra of the neat and thermo-oxidatively decomposed phosphorus additives are described in Chapter 2 (refer to section 2.4.3).

4.2.2.2.4 Hot Dip Simulation

The 55Al-43.4Zn-1.6Si coating integrity was analysed by optical microscopy and the % uncoated defect area for each sample was calculated according to the method described in Chapter 2 (refer to section 2.4.4).

4.2.3 Results and Discussion

4.2.3.1 Thermo-Oxidative Decomposition Profile

4.2.3.1.1 TGA

Figure 4.17 shows typical TGA thermo-oxidative decomposition profiles obtained for the phosphate ester (A) and amine phosphate (B) additives. A summary of the data measured from these profiles, including the onset point (T_{onset}), peak and shoulder temperatures (T_{max}) and associated mass losses, is given in table 4.9.

The phosphate ester onset point of mass loss occurs at an average value of 165 ^{o}C, within the range (150-200 ^{o}C) reported by Shankwalkar and Placek[51] for the thermo-oxidative decomposition of tri-alkyl phosphate esters. However, the T_{onset} is considerably lower than the corresponding T_{onset} values (173-231 ^{o}C) measured for triglycerides and commercial base esters in Chapter 3.2. This could be due to several factors including incomplete esterification (a broad O-H stretching band indicative of unreacted hydroxyl moieties on the phosphate head group is observed in the phosphate ester infrared spectrum; refer to figure 4.16) leading to a lower average molecular weight distribution[51] and the inferior thermo-oxidative stability of the polyethylene oxide (PEO) units contained in the phosphate ester alkyl chains; T_{onset} values determined for the thermo-oxidative decomposition of PEO-based nonionic surfactants are in the range 110-150 ^{o}C.[67, 68]

In accordance with the literature,[49-52] the phosphate ester thermo-oxidative decomposition process is dominated by two mass loss events which occur at average peak maximum temperatures of 202 ^{o}C (event 2, 40.2 % mass loss) and 263 ^{o}C (event 3, 17.4 % mass loss).

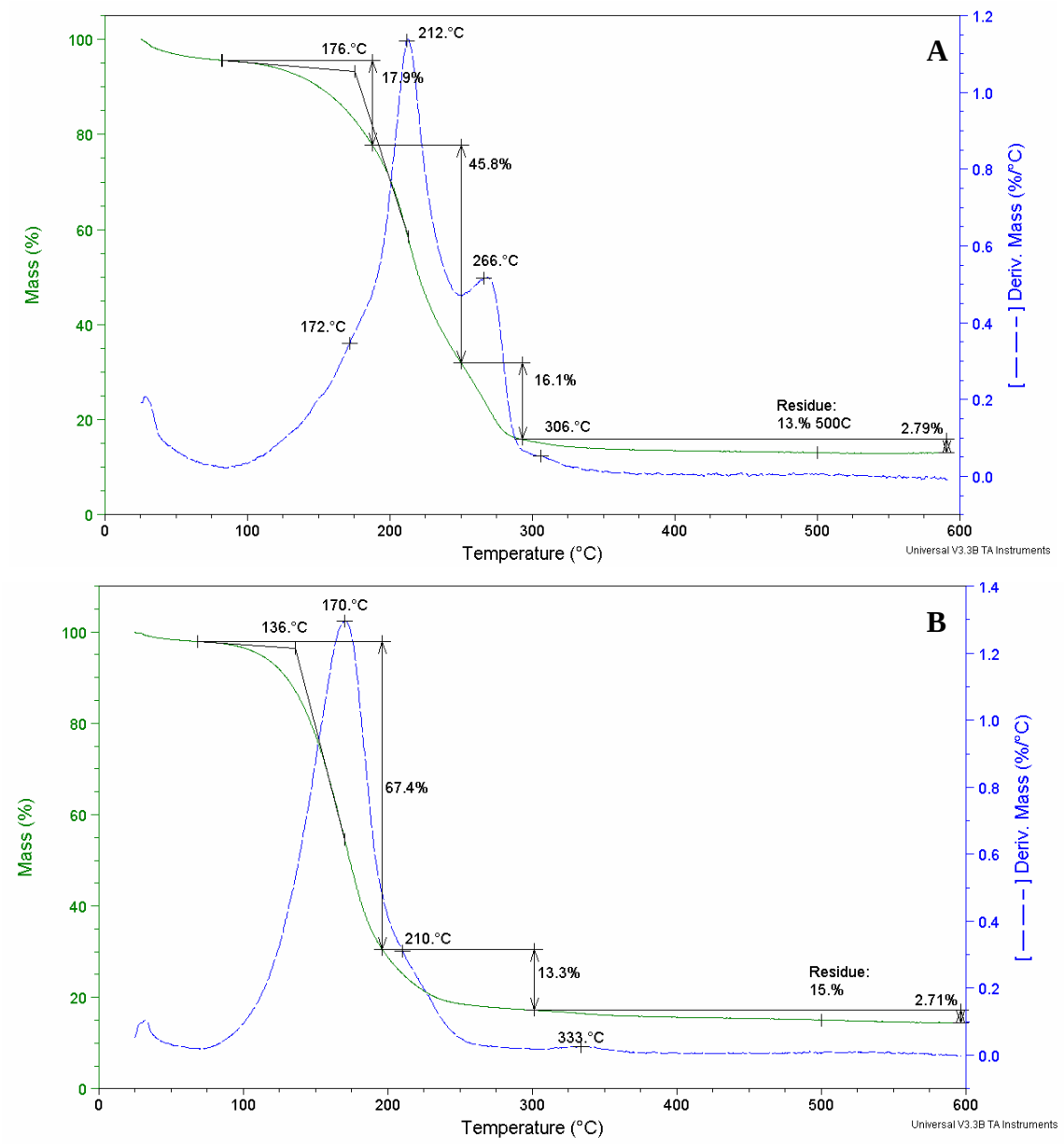

Figure 4.17 TGA thermo-oxidative decomposition profiles of the phosphate ester (A) and amine phosphate (B) additives.

These events occur at similar temperatures to events 1 and 2 observed during the thermo-oxidative decomposition of triglycerides (refer to table 3.5 in Chapter 3) and correspond to oxidative decomposition of the phosphate ester alkyl chains via the free radical mechanisms outlined by schemes 1.9-1.12 (hydroperoxide formation and decomposition) and schemes 1.14-1.16 (secondary oxidation, radical recombination and polymerisation/branching reactions to form high molecular weight products) in Chapter 1.[50, 51] As noted by Cho and Klaus,[52] the rate of phosphate ester polymerisation is much greater than the rate of formation of primary oxidation products such that significant amounts of high molecular weight deposits are likely to form during events 1 and 2.

Additional mass losses are evident immediately prior and after these events; event 1 (T_{max} = 172 ^{o}C) corresponds to a low-temperature shoulder superimposed upon event 2 and gives rise to 18.0 % mass loss. Several processes including volatilisation of low molecular weight mono- and di-phosphate esters, decomposition of PEO units in the phosphate ester alkyl chain and reaction between the phosphate head group and the aluminium pan surface could all give rise to mass loss during event 1.[51, 55, 67, 68] Furthermore, condensation reactions between unreacted hydroxyl groups on the phosphate head group may also be occurring, generating water[55] which may either volatilise or hydrolyse the ester functional groups present in the molecule. Scheme 4.3 illustrates the competing hydrolysis and condensation reactions. The phosphoric acid-type compounds produced react readily with metal cations and with one another such that additive adhesion to the aluminium pan surface and polyphosphate film formation are likely to occur simultaneously with oxidative decomposition of residual ester alkyl chains during events 2 and 3.

The final mass loss event observed during the phosphate ester thermo-oxidative decomposition process is event 4, a small, high temperature shoulder superimposed upon event 3. Event 4 occurs at peak maximum temperature of 306 ^{o}C and contributes to a mere 3.87 % mass loss up until the maximum TGA test temperature of 600 ^{o}C. This mass loss results from the thermal cracking and/or combustion of the high molecular weight char-like deposits formed by additive decomposition at lower temperatures.[49, 51]

Table 4.9 Summary of TGA and PDSC thermo-oxidative decomposition data for the two phosphorus EP additives. Errors are less than ± 10 %.

TGA											
Additive	**T_{onset} (^oC)**	**Event 1**		**Event 2**		**Event 3**		**Event 4**		**% Residue at 500 ^oC**	
		T_{max} (^oC)	**Mass Loss (%)**	**T_{max} (^oC)**	**Mass Loss (%)**	**T_{max} (^oC)**	**Mass Loss (%)**	**T_{max} (^oC)**	**Mass Loss (%)**	**O_2**	**HNX**
Phosphate Ester	165	172	18.0	202	40.2	263	17.4	306	3.87	11	8.3
Amine Phosphate	135	170	69.5	207	13.1	334	2.8	-	-	13	11
PDSC											
Additive	**T_{onset} (^oC)**	**Exotherm 1**		**Exotherm 2**		**Exotherm 3**		**Exotherm 4**		**Exotherm 5**	
		T_{max} (^oC)	**Heat Flow (Jg^{-1})**	**T_{max} (^oC)**	**Heat Flow (Jg^{-1})**	**T_{max} (^oC)**	**Heat Flow (Jg^{-1})**	**T_{max} (^oC)**	**Heat Flow (Jg^{-1})**	**T_{max} (^oC)**	**Heat Flow (Jg^{-1})**
Phosphate Ester	160	83	60.3	115	163	200	6060	277	1510	413	228
Amine Phosphate	137	175	503	206	349	309	5170	400	1240	-	-

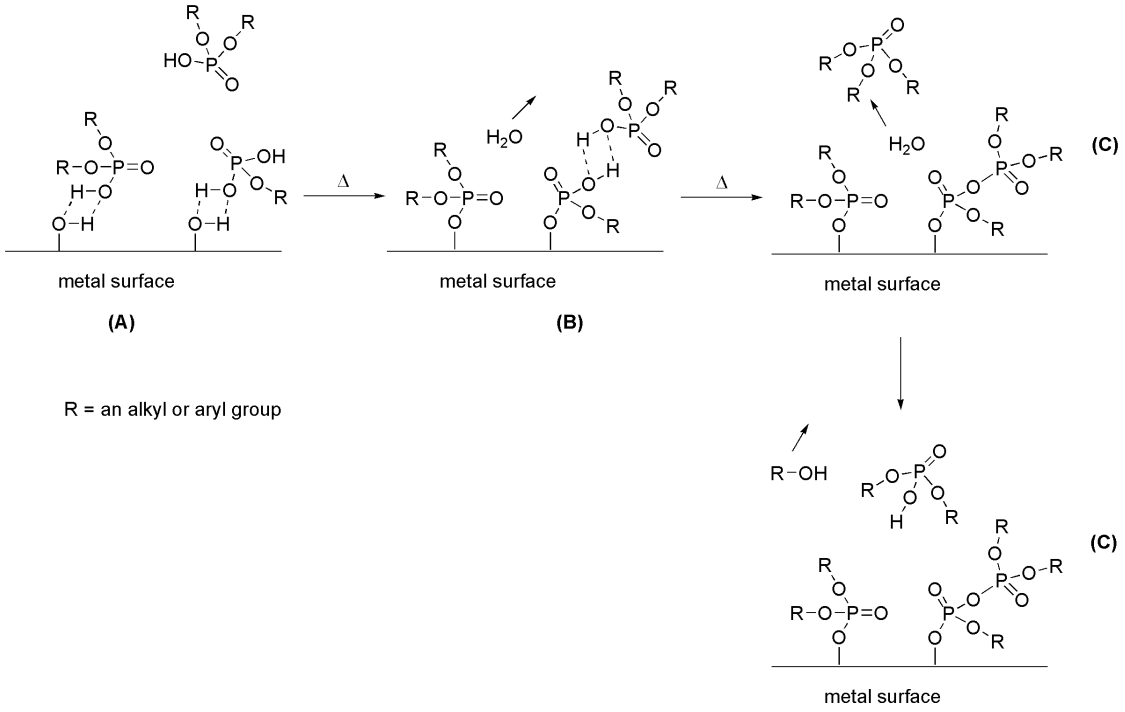

Scheme 4.3 Reactions of phosphate AW additives including A) adhesion to a metal surface, B) condensation to form a polyphosphate film and C) hydrolysis of ester functional groups.

Accordingly, a large amount of residue is present at 500 ^{o}C (~ 11 %). This level of residue exceeds both the amount of phosphorus contained in the additive (~ 4.7 % w/w) and the percentage of sample mass attributable to the phosphate head group (~ 6.3 %) and is likely to comprise of residual carbonaceous material ('char') in addition to bound polyphosphate and/or phosphide compounds.[55, 57-60, 62] Furthermore, 8.3 % residue remains at 500 ^{o}C after decomposition of the phosphate ester under thermo-reductive (HNX) conditions. This indicates that although oxidised deposits contribute to the amount of residue remaining after the phosphate ester thermal decomposition process, residue composition is largely unaffected by the use of thermo-reductive as opposed to thermo-oxidative conditions.

The amine phosphate is less thermo-oxidatively stable than phosphate ester as evidenced by its lower average T_{onset} value of ~ 135 ^{o}C. Although this appears to contradict the

findings reported in the literature (aryl phosphates have been shown to possess superior resistance towards oxidative degradation than alkyl phosphate derivatives),[49, 51, 53] the amine phosphate is a di-functional phosphate ester whereas the phosphate ester is tri-functional. Therefore, the greater volatility of the amine phosphate is likely to result from its lower molecular weight.[51]

Although the event 1 and 2 T_{max} values measured for the amine phosphate (170 ^{o}C and 207 ^{o}C respectively) are approximately the same as for events 2 and 3 observed for the phosphate ester, the comparable proportions of mass loss differ, with event 1 representing the majority of amine phosphate mass loss (69.5 %) and event 2 (observed as a high temperature shoulder on event 1) contributing a mere 13.1 % mass loss. This is due to the different chemical composition of the amine phosphate additive. The infrared spectrum shown in figure 4.16 indicates that the amine phosphate contains less free hydroxyl functional groups than the phosphate ester as the broad O-H stretching band at ~ 3368 cm^{-1} is significantly lower in intensity. Therefore, the hydrolysis and condensation reactions which give rise to polyphosphate film formation during event 1 during the phosphate ester thermo-oxidative decomposition process occur less readily in the amine phosphate. A greater proportion of event 1 mass loss therefore results from sample evaporation and/or oxidative decomposition as opposed to condensation and the hydrolytic loss of alkyl functional groups.

Fewer volatiles are evolved by the secondary oxidation reactions undergone by the amine phosphate during event 2. In addition, the residues formed by these reactions are more thermally stable than the analogous residues formed by decomposition of the phosphate ester; event 3 observed for the amine phosphate occurs at a peak temperature of 334 ^{o}C and contributes to only 2.8 % mass loss. Consequently, the amine phosphate thermo-oxidatively decomposes to form a greater amount of residue (~ 13 %) at 500 ^{o}C. The composition of this residue is analogous to that of the phosphate ester residue, however it may contain ammonium phosphate-type compounds.[58, 62] As noted for the phosphate ester, the amount of residue detected at 500 ^{o}C after decomposition of the amine phosphate under HNX (11 %) is ~ 2 % less than under oxygen.

Despite the incorporation of phosphate AW additives at low concentrations in commercial cold rolling oils (typically 1-2 % w/w), the levels of residue formed by phosphate additive thermo-oxidative decomposition exceed those formed by sulfurised triglyceride EP additives (refer to table 4.2). Further investigation into the impact of phosphate AW additive residues on metallic coating quality is therefore warranted.

4.2.3.1.2 PDSC

Constant-volume PDSC analysis of the two phosphorus additives yields the heat flow vs. temperature plots shown in figure 4.18. The onset point (T_{onset}), peak and shoulder temperature (T_{max}) and respective enthalpy values determined from the curves are summarised in table 4.9 above.

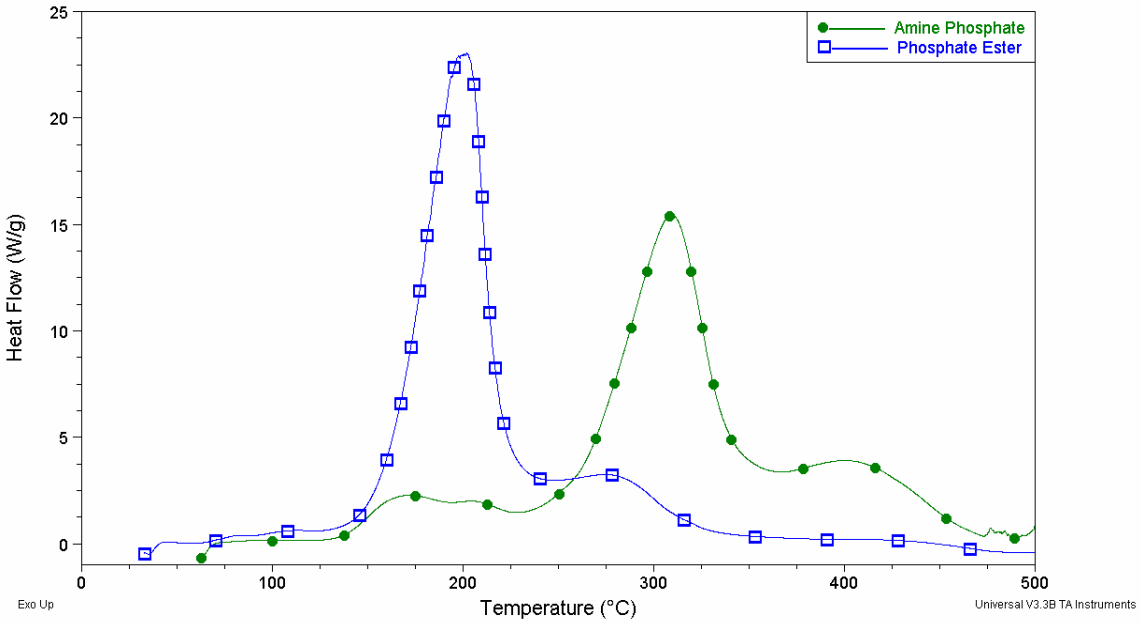

Figure 4.18 Overlay of the PDSC thermo-oxidative decomposition profiles of the phosphate ester and amine phosphate.

The PDSC T_{onset} value measured for the phosphate ester is 160 ^{o}C, ~ 5 ^{o}C below the corresponding T_{onset} measured by TGA. This is in good agreement with the findings of

Shankwalkar et al.[51] and confirms that the initial stages of phosphate ester TGA mass loss result from oxidative decomposition as opposed to evaporation. A total of five overlapping net exothermic events are observed in the phosphate ester PDSC thermogram shown in figure 4.18. The first two of these exotherms occur at average T_{max} values of 83 ^{o}C (exotherm 1) and 113 ^{o}C (exotherm 2) and correspond to a mere 0.75 and 2.0 % of the total heat flow respectively. Du et al.[65] observed small, sharp exotherms prior to the main oxidation peak during the PDSC analysis of zinc dithiocarbamate/base oil blends and attributed these exotherms to the formation of primary oxidation products. However, the exotherms observed in the current investigation are broad in appearance and are therefore likely to indicate reaction of between the phosphate head group with the aluminium pan surface and the subsequent commencement of ester hydrolysis and condensation reactions.[55, 57]

Exotherm 3 (T_{max} = 200 ^{o}C) is the major exothermic event observed during the phosphate ester thermo-oxidative decomposition process, accounting for ~ 76 % of the total heat flow. It occurs at a similar temperature and is similar in profile to exotherm 1 observed for coconut oil and commercial base esters (refer to Chapter 3) and therefore represents simultaneous oxidation, thermal cracking and combustion of the hydrocarbon portion of the additive. Accordingly, decomposition of residual high molecular weight/oxidised deposits occurs during event 4 at ~ 277 ^{o}C (19 % of the total heat flow).

The final exotherm observed during the phosphate ester thermo-oxidative decomposition process is exotherm 5, which occurs at a peak maximum temperature of 413 ^{o}C and accounts for 2.8 % of the total heat flow. In accordance with the findings of Perez et al.[59] for the oxidative decomposition of tricresyl phosphate, exotherm 5 represents the formation of a polyphosphate glass-like material.

Although PDSC results in table 4.10 show that the amine phosphate exhibits a lower oxidative stability than the phosphate ester (T_{onset} occurs at 137 ^{o}C, ~ 23 ^{o}C below that of the phosphate ester), the fact that its PDSC T_{onset} is greater than the T_{onset} value measured by TGA confirms that the initial stages of amine phosphate mass loss result from evaporation as opposed to oxidative decomposition.[49, 51, 53]

Four exothermic events are apparent in the amine phosphate PDSC curve shown in figure 4.18. The first two occur at peak maximum values of 175 ^{o}C and 206 ^{o}C and give rise to ~ 6.9 % and 4.8 % of the total heat flow respectively. These exotherms are analogous to the first two exotherms observed for the phosphate ester and represent additive adhesion the aluminium pan surface together with hydrolysis and condensation reactions.[55, 57] The fact that these reactions occur at higher temperatures for the amine phosphate than for the phosphate ester is in agreement with the FTIR and TGA results described above.

Exotherm 3 occurs at ~ 309 ^{o}C and gives rise to the majority of the total heat flow (71 % or 5170 J g^{-1}). This exotherm indicates the commencement of the oxidative decomposition reactions outlined above for the phosphate ester and it occurs at higher temperature than events 1 and 2 noted by TGA, suggesting that very little amine phosphate mass loss results from oxidative decomposition.[49, 51, 53] Exotherm 4 at 400 ^{o}C (~ 17 % of the total heat flow) indicates formation of high molecular weight deposits and the small exothermic peaks observed following exotherm 4 (at 475-490 ^{o}C) are analogous to those observed during the oxidation of cottonseed oil in Chapter 3.2 and indicate the commencement of thermal cracking reactions. The amine phosphate thermo-oxidative decomposition process by PDSC is incomplete at 500 ^{o}C, accounting for the significant amount of residue detected by TGA.

4.2.3.2 ATR Characterisation of Additive Residues

In order to characterise the chemical nature of the residues remaining after thermo-oxidative decomposition of the phosphate ester and amine phosphate additives, mid-infrared ATR analysis was performed. Figure 4.19 shows the spectra obtained in the region 1450-600 cm^{-1} (the absence of absorptions in the range 4000-1400 cm^{-1} confirms the decomposition of the hydrocarbon portions of the additives) and the peak assignments for these spectra are detailed in table 4.10.

There is little difference between the two spectra shown in figure 4.19, suggesting that the residues formed by thermo-oxidative decomposition of the phosphate ester and

amine phosphate additives possess similar chemical composition. Significant evidence of phosphorus-containing functional groups is present in the spectra. Bands at 766 cm^{-1} and 768 cm^{-1} can be attributed to the P-O-C stretching vibration in organo-oxy-phosphorus compounds or the symmetrical O-P-O stretching vibration associated with the oxygen-phosphorus backbone in short-chain $(-O-P-)_n$ compounds such as orthophosphates.[60] The broadness of these bands is consistent with the findings of Willermet et al.[60] for the thermo-oxidative decomposition of a zinc dialkyl dithiophosphate/base oil blend, and suggests an amorphous residue structure.

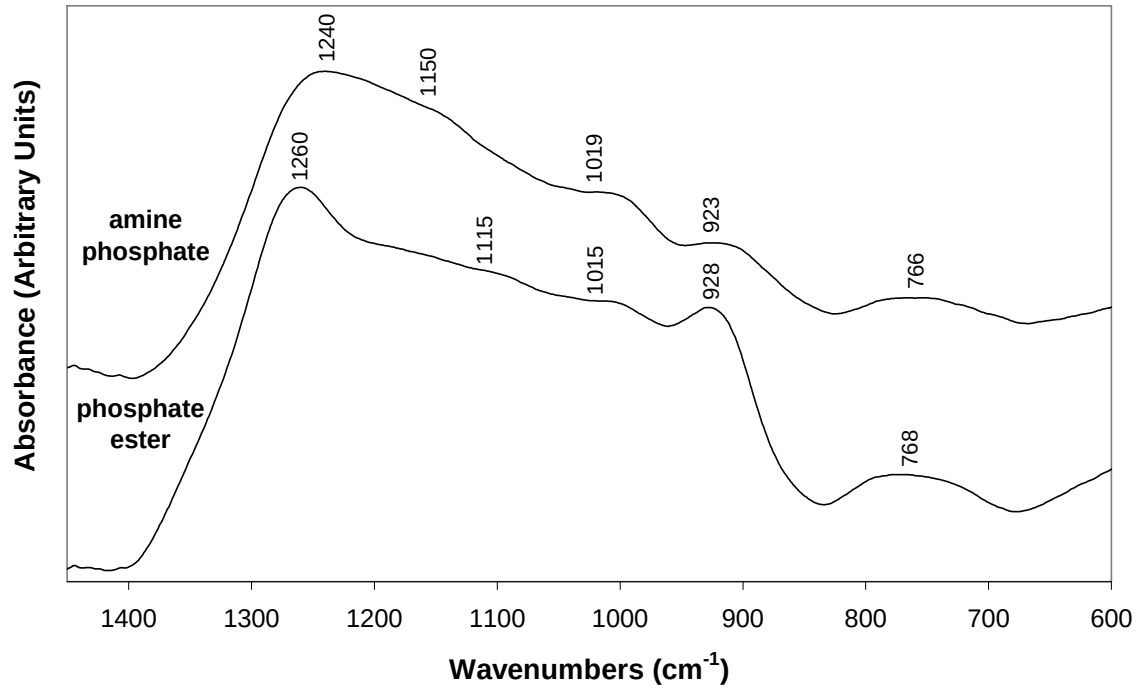

Figure 4.19 ATR spectra of residues remaining after thermo-oxidative decomposition of the phosphate ester and amine phosphate additives at 500 °C.

Bands at 928 cm^{-1} and 923 cm^{-1} have been associated with the stretching absorptions of numerous different phosphorus-containing groups, including P-O-C,[59, 66, 69] P=O,[66] O-P-O[60] and P-O-P.[32] Similarly, the broad bands observed at ~ 1019 cm^{-1} and 1015 cm^{-1} are typical of the P-O-C and/or O-P-O stretching vibrations[32, 59, 65, 66] whilst bands in the

region 1260-1100 cm^{-1} are due to P=O stretching modes in PO_2^- or to C-O stretching in C-O-C.[32, 59, 60, 65]

Table 4.10 Peak assignments for phosphate ester and amine phosphate thermo-oxidative decomposition residue spectra.[32, 59, 60, 65, 66]

Peak (cm^{-1})		Assignment
Phosphate Ester	**Amine Phosphate**	
1260	1240	νP=O; νPO_2^- (asym.); νC-O in C-O-C
-	1150	νPO_2^- (sym.); νC-O in C-O-C
1115	-	νPO_2^- (sym.); νC-O in C-O-C
1015	1019	νP-O-C; νO-P-O (asym.)
928	923	νP-O-C; νP=O; νO-P-O (asym.); νP-O-P
768	766	νO-P-O (sym.)

ν = stretching

asym. = asymmetrical; sym. = symmetrical

Given that the additives in the present study are not blended with base oils, any residues containing P-O-C or C-O-C functionalities must be derived from the additive structure itself. Furthermore, the absence of C-H stretching vibrations in the region 3000-2800 cm^{-1} suggests that a limited amount of hydrocarbon-based compounds are present. These factors infer that the residues formed by thermo-oxidative decomposition of the phosphate ester and amine phosphate additives comprise of amorphous oxygenated carbon deposits containing phosphate moieties such as orthophosphates, pyrophosphates and small amount of short chain $(\text{-O-P-})_n$ compounds.[59, 60] This residue composition is in good agreement with findings made for the thermo-oxidative decomposition of phosphorus anti-wear additives using other chemical analysis techniques.[6, 58, 61] The lack of absorptions characteristic of nitrogen-containing functional groups (such as ammonium ions ~ 3300-3030 cm^{-1}) in the amine phosphate residue spectrum is

consistent with the findings of Najman et al.,[58] who determined that a commercial amine phosphate additive decomposed under EP conditions to form a iron polyphosphate as opposed to an ammonium polyphosphate. No carboxylate, carbonyl-based or aromatic products are detected such that the chemical composition of the phosphorus additive residue differs significantly to that formed by the triglycerides and commercial base esters studied in Chapter 3.2 and the sulfur-based EP additives described in section 1 of this Chapter.

4.2.3.3 Effect of Phosphorus EP Additive Chemical Structure and Concentration on Base Ester Residue Levels

The effect of the phosphate ester and amine phosphate additives on the residue-forming tendency of commercial base ester A can be determined by calculating the % B/A ratio from TGA and PDSC data according to equation 3.1 in Chapter 3.[27, 28] The temperature ranges over which the primary (A) and secondary (B) decomposition regions are defined are the same as in Chapter 3 and section 1 of this Chapter; mass loss and heat flow events in the range 300-500 ^{o}C are included within 'B' and those occurring between room temperature and 300 ^{o}C are included within 'A'. Figure 4.20 shows a plot of the PDSC and TGA % B/A ratios determined for blends of each of the additives in ester A at 0.05 % w/w and 2.5 % w/w phosphorus concentration. These two concentration levels represent the typical phosphorus concentration employed in commercial cold rolling oil formulations and high phosphorus concentration respectively.

At both of the phosphorus concentration levels studied, the additives increase the deposit-forming tendency of commercial base ester A. At 0.05 % w/w phosphorus concentration, the amine phosphate increases the PDSC % B/A ratio to 3.4 %, a value which is almost twice the PDSC % B/A ratio of neat ester A (1.8 %). A similar increase in noted for the phosphate ester (PDSC % B/A ratio = 3.2 %). These results are consistent with the findings of others[52, 62] and suggest that even at low phosphorus concentration, the additives promote the formation of residues that decompose to evolve proportionately more energy than the residues formed by ester A alone.

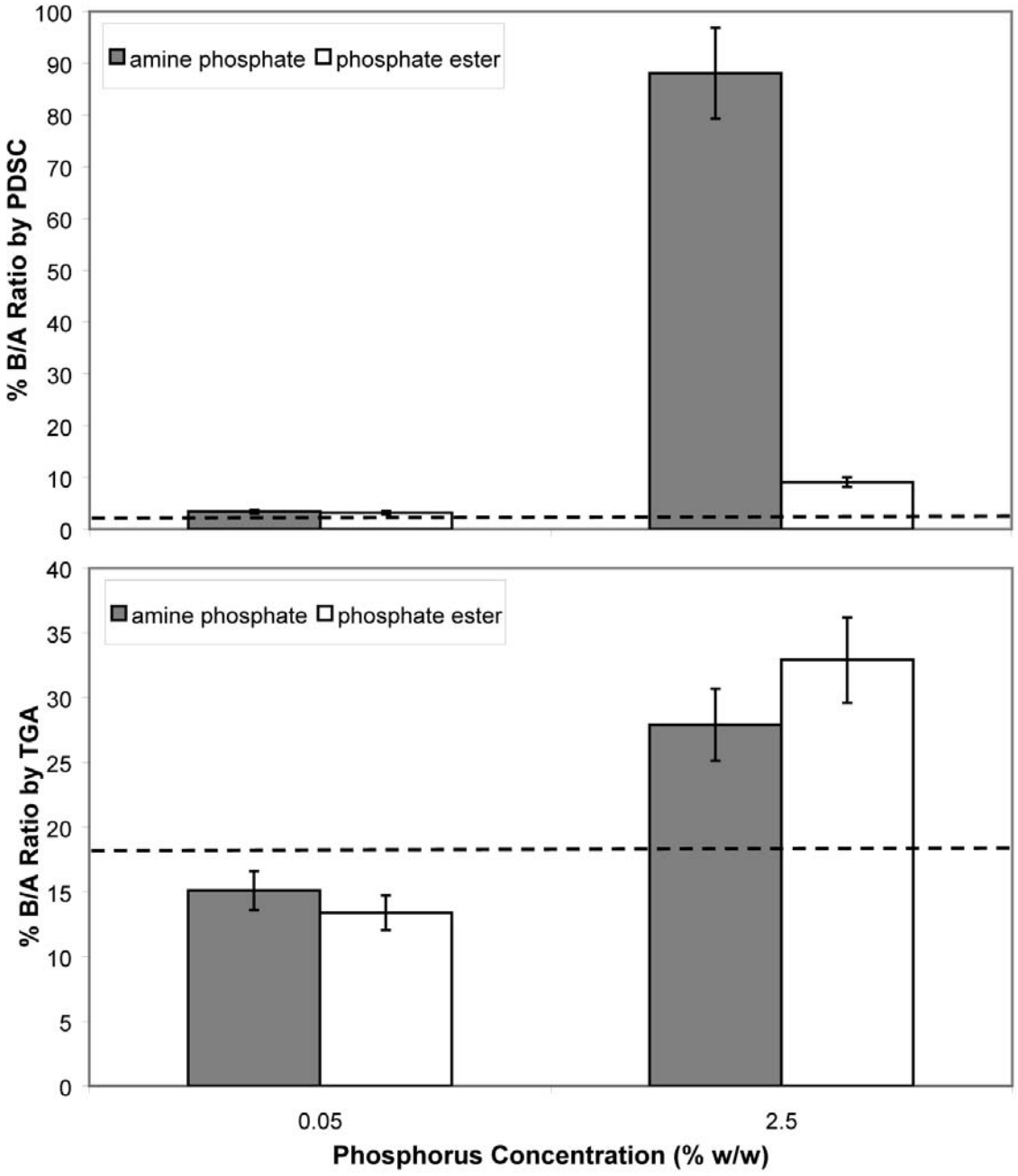

Figure 4.20 Plots of the TGA and PDSC % B/A ratios determined for blends of the amine phosphate and phosphate ester in base ester A at 0.05 and 2.5 % w/w phosphorus concentration. The error bars represent ± 10 % error. The dashed lines indicate the neat ester A % B/A ratio (1.6 % by PDSC; 18 % by TGA).

As noted by Adhvaryu et al.[62] and Willermet et al.,[55] these residues are likely to consist of intermediates formed by reactions between base ester oxidation products (such as radical species, alcohols and carboxylic acids) and either the phosphate ester alkyl chains or free hydroxyl moieties present on the phosphate head group (scheme 4.4). The base ester-derived alkyl chains may subsequently oxidise and polymerise to form high molecular weight branched and/or networked deposits.

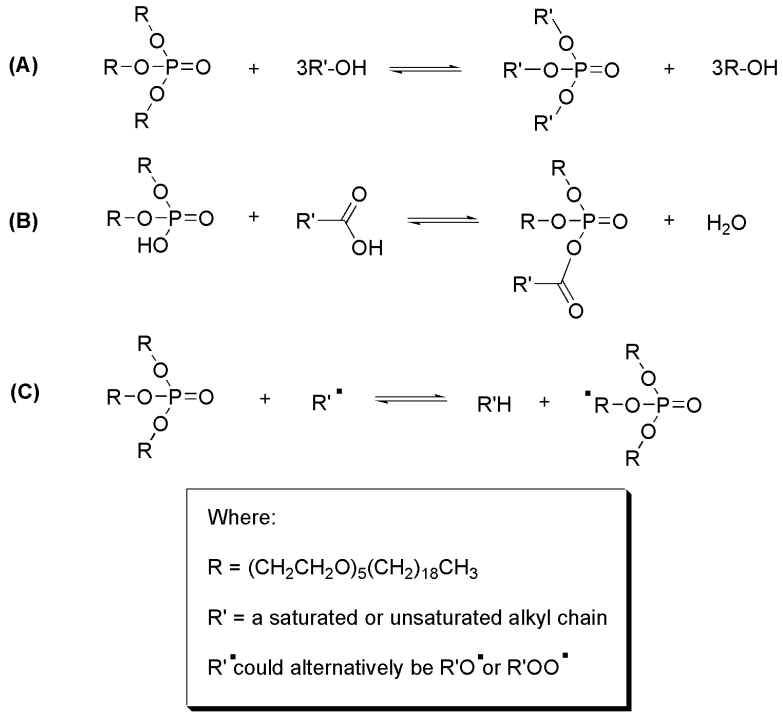

Scheme 4.4 Reactions between base ester oxidation products and the phosphate ester including transesterification (A), esterification (B) and radical propagation (C; note that hydrogen abstraction occurs most readily at the α carbon position in the ethoxylated portion of the alkyl chain[68]).

In contrast to the PDSC results, the TGA % B/A ratios determined for the amine phosphate and phosphate ester blends at 0.05 % w/w phosphorus concentration are 15 % and 13 % respectively, below the corresponding value for neat ester A (18 %). This confirms that the residue formed by the phosphorus additive/ester A blends is less volatile than the residue formed by decomposition of ester A alone. Accordingly, the

increase in the PDSC % B/A ratio is caused by a change in the chemical composition of the residue as opposed to the decomposition of greater amounts of residue.

At 2.5 % w/w phosphorus concentration, both the PDSC and TGA % B/A ratio values determined for the additive/ester A blends increase dramatically. The phosphate ester blend yields % B/A ratio values of 9.1 % (PDSC) and 33 % (TGA) whilst the corresponding values calculated for the amine phosphate are 88 % (PDSC) and 28 % (TGA). Therefore, although the increase in TGA % B/A ratio going from 0.05 % w/w to 2.5 % w/w phosphorus concentration is relatively consistent between the two additives, the increase in the PDSC % B/A ratio for amine phosphate blend is more dramatic. This is due to a shift in the temperature at which oxidative decomposition reactions occur to significantly higher value and is reflected by a considerable increase in the PDSC onset temperature of oxidation from 200 ^{o}C (neat ester A) to 217 ^{o}C at 0.05 % w/w phosphorus concentration and 252 ^{o}C at 2.5 % w/w phosphorus concentration. The amine phosphate therefore displays an anti-oxidant effect and increases the oxidative stability of ester A, resulting in dramatic increase in the heat flow measured over the secondary (B) decomposition region. The phosphate ester % B/A ratio results at 2.5 % w/w phosphorus concentration show an approximately two-fold increase in the % B/A ratio by both PDSC and TGA. This implies that the increased energy evolved by residue decomposition results from the decomposition of a greater amount of residue (the chemical composition of this residue may or may not be the same as at 0.05 % w/w phosphorus concentration).

A comparison between the phosphorus additive % B/A ratio results with those determined for sulfurised EP additives in section 1 of this Chapter reveals that whilst the two types of additives produce similar TGA % B/A ratio results at 2.5 % w/w phosphorus or sulfur concentration, the PDSC % B/A ratio determined for phosphorus additive blends is comparable to that observed for the sulfurised additive blends at 0.1 % w/w sulfur concentration. This suggests that the sulfurised additives increase the residue-forming tendency of ester A to a much greater extent than do the phosphorus-based additives.

4.2.3.4 Residue Impact on 55Al-43.4Zn-1.Si Coating Quality

The impact of the phosphate ester and amine phosphate residues on 55Al-43.4Zn-1.6Si coating quality has been assessed by performing hot dip metallic coating simulations using steel samples treated with blends of each of the additives at 2.5 % w/w phosphorus concentration in commercial base ester A. Figure 4.21 shows optical microscopy images of the resultant 55Al-43.4Zn-1.6Si coated samples.

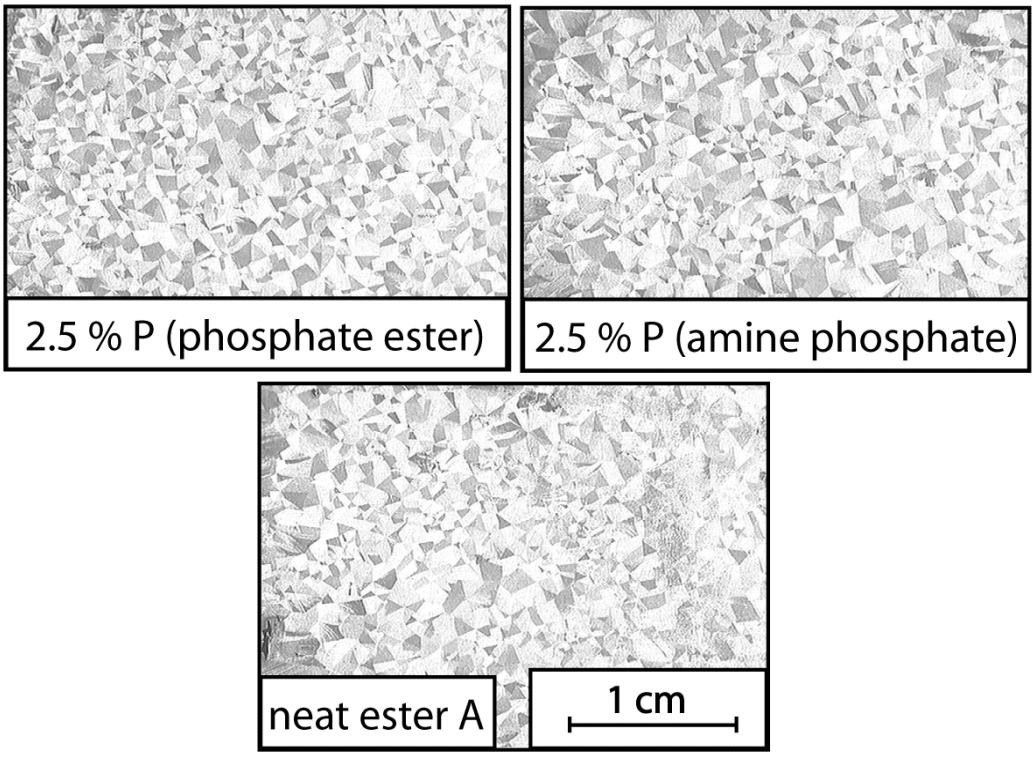

Figure 4.21 Optical microscopy images of 55Al-43.4Zn-1.6Si coated steel samples prepared using the hot dipping simulator after the application of blends of the phosphate ester and the amine phosphate at 2.5 % w/w phosphorus concentration in base ester A. A control sample prepared from steel treated with neat ester A is shown for comparison.

The coating results show that neither of the phosphorus-based additives impacts detrimentally upon metallic coating quality relative to ester A. On the contrary, the

coating quality appears to improve with the addition of the additives; the amine phosphate and phosphate ester-treated samples possess fewer uncoated defects than the neat base ester A-treated sample. This is confirmed by figure 4.22, which compares the % uncoated defect areas calculated for the three samples.

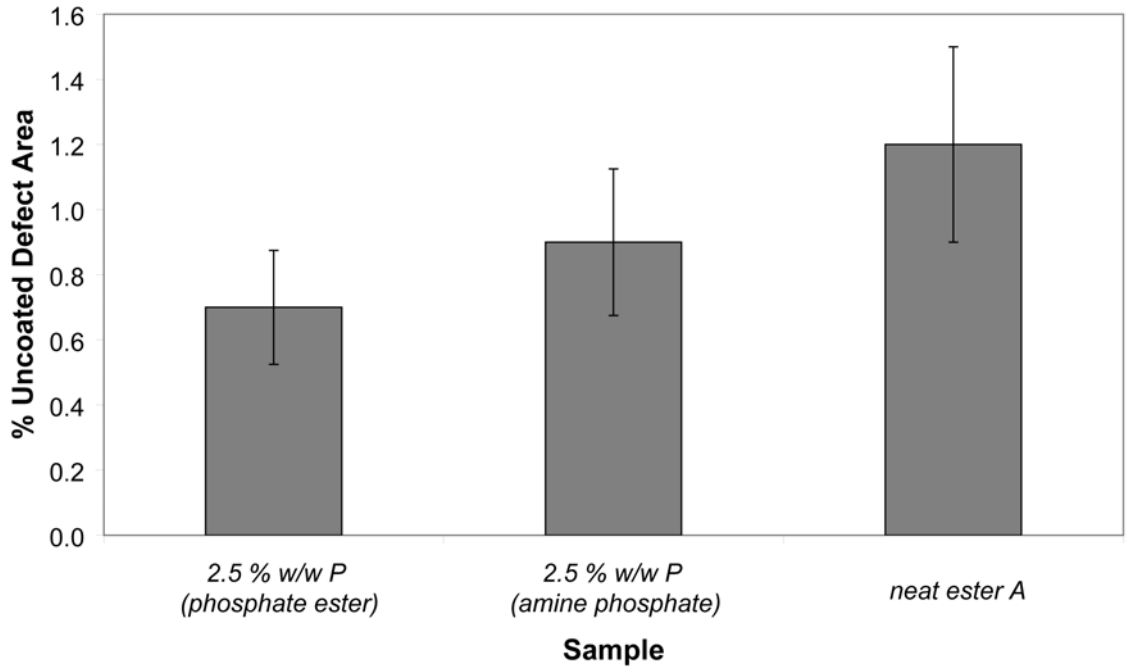

Figure 4.22 % uncoated defect area results determined for 55Al-43.4Zn-1.6Si coated samples prepared from steel treated with blends of the phosphate ester and amine phosphate in base ester A at 2.5 % w/w phosphorus concentration and neat ester A. The error bars represent ± 25 % error.

Although the % uncoated defect area results determined for the three samples are within experimental error margins, a qualitative comparison shows that the addition of the additives at 2.5 % w/w phosphorus concentration results in a decrease in the % uncoated defect area from 1.2 % to 0.9 % and 0.7 % for the amine phosphate and phosphate ester blends respectively. This suggests that despite the significant amount of residue formed by decomposition of the phosphorus-based additives (11-13 % under oxygen; 8.3-11 % under HNX) and their blends, this residue does not affect the steel surface wettability by

the molten coating alloy. This beneficial effect could result from competition between the additives and ester A for binding sites at the steel surface.[58, 61] Preferential adsorption of the additives could prevent the formation of the carboxylate-based residues which have been shown to have a detrimental effect on coating quality in Chapters 3 and 5. Furthermore, oxidation of the phosphorus-based additives may be more favourable, minimising the formation of oxidised oil deposits.[59] In addition to these factors and in accordance with the ATR results presented above, the residue formed by decomposition of the phosphorus-based additives has a different chemical composition to that formed by the sulfur EP additives. The impact of the two kinds of residue on the steel surface energy, and therefore on intermetallic layer formation and steel surface 'wettability' by the molten alloy, is likely to differ and could account for the non-deleterious effect of the phosphorus-based additives on metallic coating quality.[10, 11, 45]

4.2.4 Conclusions

TGA analysis of phosphate ester and amine phosphate anti-wear additives under both thermo-oxidative and –reductive atmospheres shows that the additives decompose to leave significant amounts (> 10 % w/w) of thermally-stable residue at 500 ^{o}C. Infrared characterisation of this residue reveals that it comprises of short-chain organically-bound polyphosphates and oxidised carbonaceous material. Both additives increase the amount and change the chemical composition of the residue formed by thermo-oxidative decomposition of a commercial base ester as determined by the % B/A ratio technique. However, hot dipping simulation results show that blends of each additive at high (2.5 % w/w phosphorus) concentration in a commercial base ester do not impact detrimentally upon 55Al-43.4Zn-1.6Si coating quality. The potential therefore exists for optimising phosphorus-based additive concentration in commercial cold rolling oils to achieve enhanced rolling capability and developing phosphorus EP/AW additives as replacements for sulfurised additives.

4.3 References

1. Kim, S. M., Sit, C. Y., Komvopoulos, K., Yamaguchi, E. S., Ryason, P. R., *Tribol. Trans.* **2000,** *43*, 569.

2. Qiu, C., Han, S., Cheng, X., Ren, T., *Thermochim. Acta* **2006,** *447*, 36.

3. Najman, M. N., Kasrai, M., Bancroft, G. M., *Tribol. Lett.* **2003,** *14*, 225.

4. Lara, J., Blunt, T., Kotvis, P., Riga, A., Tysoe, W. T., *J. Phys. Chem. B* **1998,** *102*, 1703.

5. Bala, V., Hartley, R. J., Hughes, L. J., *Lubr. Eng.* **1996,** *52*, 868.

6. Komvopoulos, K., Do, V., Yamaguchi, E. S., Yeh, S. W., Ryason, P. R., *Tribol. Trans.* **2004,** *47*, 321.

7. Morris, R. E., Mushrush, G. W., *Prepr. Pap. - Am. Chem. Soc., Div. Fuel Chem.* **1989,** *34*, 538.

8. Fabuss, B. M., Duncan, D. A., Smith, J. O., Satterfield, C. N., *Ind. Eng. Chem. Proc. Des. Dev.* **1965,** *4*, 117.

9. Keyser, A. G., Kunkel, K. F., Snedaker, L. A., *Iron Steel Eng.* **1998,** *75*, 43.

10. Tang, N.-Y., Goodwin, F. E. In *A study of defects in galvanized coatings*, Galvatech '01 - Proc. 5th Int. Conf. on Zinc and Zinc Alloy Coated Steel Sheet, Brussels, Belgium; 2001, pp 49.

11. Chen, F., Patil, R. In *An in-depth analysis of various subtle coating defects of the 2000's*, Galvatech '04 - Proc. 6th Int. Conf. on Zinc and Zinc Alloy Coated Steel Sheet, Chicago, USA; 2004, pp 1055.

12. Ahmad, L. A., Eissa, E. A., Taman, A. R., *Erd. Koh. Erdg. Petr. V.* **1991,** *44*, 151.

13. Sech, J. M., Oleksiak, T. P., *Iron Steel Eng.* **1995,** *72*, 33.

14. Guanteng, G., Spikes, H. A., *Tribol. Trans.* **1996,** *39*, 448.

15. Le, H. R., Sutcliffe, M. P. F., *Tribol. Trans.* **2001,** *44*, 284.

16. Lin, H. S., Marsault, N., Wilson, W. R. D., *Tribol. Trans.* **1998,** *41*, 317.

17. Riga, A. T., Hong, H., Kornbrekke, R. E., Cahoon, J. M., Vinci, J. N., *Lubr. Eng.* **1992,** *49*, 65.

18. Colclough, T., *Ind. Eng. Chem. Res.* **1987,** *26*, 1888.

19. Martin, G., Pyrolysis of organosulfur compounds. In *The chemistry of sulfur-containing functional groups*, Patai, S., 'Ed."; John Wiley and Sons Ltd: 1993; pp 395.
20. Voronkov, M. G., Deryagina, E. N., Thermal reactions and high temperature syntheses of organosulfur compounds. In *Chemistry of Organosulfur Compounds: General Problems*, Belen'kii, L. I., 'Ed."; Ellis Horwood: New York, 1990; pp 48.
21. Akiba, M., Hashim, A. S., *Prog. Polym. Sci.* **1997,** *22*, 475.
22. Gonzalez, L., Rodriguez, A., Del Campo, A., Marcos-Fernandez, A., *J. Appl. Polym. Sci.* **2002,** *85*, 491.
23. Hasenhuettl, G. L., Fats and Fatty Oils. In *Kirk-Othmer Encyclopedia of Chemical Technology*, Kroschwitz, J. I., 'Ed."; John Wiley & Sons: New York, 2005; pp 801.
24. Sundarrajan, S., Surianarayanan, M., Srinivasan, K. S. V., *J. Polym. Sci., Part A: Polym. Chem.* **2005,** *43*, 638.
25. Oyman, Z. O., Ming, W., van der Linde, R., *Prog. Org. Coat.* **2005,** *54*, 198.
26. Frankel, E. N., *Prog. Lipid Res.* **1985,** *23*, 197.
27. Zhang, Y., Perez, J. M., Pei, P., Hsu, S. M., *Lubr. Eng.* **1992,** *48*, 221.
28. Zhang, Y., Pei, P., Perez, J. M., Hsu, S. M., *Lubr. Eng.* **1992,** *48*, 189.
29. Gamlin, C. D., Dutta, N. K., Choudhury, N. R., Kehoe, D., Matisons, J., *Thermochim. Acta* **2002,** *392-393*, 357.
30. Gines, M. L. J., Benitez, G. J.,Perez, T., Bossi, E. In *Surface reactions during batch annealing process*, Proc. 55th Annual ABM Congress, Rio de Janeiro; 2000, pp 2239.
31. Suilen, F., Zuurbier, S. In *Fundamental aspects of gas-metal reactions during batch annealing in 100% hydrogen*, Proc. 38th Mechanical Working and Steel Processing Conference, Ohio, USA; 1997, pp 375.
32. Williams, D. H., Fleming, I., *Spectroscopic Methods in Organic Chemistry*. 5 ed.; McGraw-Hill Publishing Company: England, 1997.
33. Szymanski, H. A., *Infrared Band Handbook*. Plenum Press: New York, 1963.
34. Vogel, A. I., Tatchell, A. R., Furnis, B. S., Hannaford, A. J., Smith, P. W. G., *Vogel's Textbook of Practical Organic Chemistry, 5th edition*. Addison Wesley Longman Ltd: London, UK, 1989.

35. Block, E., Ahmad, S., Catalfamo, J. L., Jain, M. K., Apitz-Castro, R., *J. Am. Chem. Soc.* **1986,** *108*, 7045.

36. Solomons, T. W. G., Fryhle, C. B., *Organic Chemistry, 7th edition*. John Wiley and Sons, Inc.: New York, 2000.

37. Hanaki, K., *Sumimoto Light M. Tech.* **1984,** *25*, 44.

38. Singh, C., Upadhyaya, S. K., *Asian J. Chem.* **2001,** *13*, 977.

39. Upadhyaya, S. K., Sharma, P. S., *Asian J. Chem.* **1997,** *9*, 388.

40. Abou El Naga, H. H., Salem, A. E. M., *Wear* **1984,** *96*, 267.

41. Nakamoto, K., *Infrared and Raman Spectra of Inorganic and Coordination Compounds, 4th Edition*. 4th ed.; John Wiley and Sons, Inc.: New York, 1986.

42. Nyquist, R. A., Kagel, R. O., *Infrared Spectra of Inorganic Compounds (3800 - 45cm^{-1})*. Academic Press: New York, 1971.

43. Reusch, W. Infrared Spectroscopy. http://www.cem.msu.edu/~reusch/VirtualText/Spectrpy/InfraRed/infrared.htm (30/05/07).

44. Domalski, E. S., *J. Phys. Chem. Ref. Data* **1972,** *1*, 221.

45. Browne, K. M., *Zincalume pinhole uncoated investigation: progress report*; 726; John Lysaght (Australia) Limited: April, 1980; pp 1.

46. Willem, J.-F., Claessens, S., Cornil, H., Fiorucci, M., Hennion, A., Xhoffer, C. In *Solidification mechanisms of aluzinc coatings - effect on spangle size*, Galvatech '01 - Proc. 5th Int. Conf. on Zinc and Zinc Alloy Coated Steel Sheet, Brussels, Belgium; 2001, pp 401.

47. Hendrix, J. E., Drake, G. L., *J. Appl. Polym. Sci.* **1972,** *16*, 257.

48. Huang, M.-R., Li, X. -G., *J. Appl. Polym. Sci.* **1998,** *68*, 293.

49. Shankwalkar, S. G., Cruz, C., *Ind. Eng. Chem. Res.* **1994,** *33*, 740.

50. Kettrup, A., Ohrbach, K. -H., Matuschek, G., Joachim, A., *Thermochim. Acta* **1990,** *166*, 41.

51. Shankwalkar, S. G., Placek, D. G., *Ind. Eng. Chem. Res.* **1992,** *31*, 1810.

52. Cho, L., Klaus, E. E., *ASLE Trans.* **1981,** *24*, 119.

53. Shankwalkar, S. G., Placek, D.G., *J. Synth. Lubr.* **1994,** *11*, 121.

54. Gschwender, L. J., Snyder, C. E., Fultz, G. W., Chen, L. S., *Lubr. Eng.* **1991,** *47*, 935.

55. Willermet, P. A., Dailey, D. P., Carter III, R. O., Schmitz, P. J., Zhu, W., *Tribol. Int.* **1995,** *28*, 177.

56. Han, S.-Y., Yi, J. -J., *ISIJ Int.* **1997,** *37*, 498.

57. Komatsuzaki, S., Nakano, F., Uematsu, T., Narahara, T., *Lubr. Eng.* **1985,** *41*, 543.

58. Najman, M. N., Kasrai, M., Bancroft, G. M., *Wear* **2004,** *257*, 32.

59. Perez, J. M., Ku, C. S., Pei, P., Hegemann, B. E., Hsu, S. M., *Tribol. Trans.* **1990,** *33*, 131.

60. Willermet, P. A., Carter III, R. O., Boulos, E. N., *Tribol. Int.* **1992,** *25*, 371.

61. Arezzo, F., *ASLE Trans.* **1985,** *28*, 203.

62. Adhvaryu, A., Erhan, S. Z., Perez, J. M., *Wear* **2004,** *257*, 359.

63. Ma, Y., Liu, J., Zheng, L., *Tribol. Int.* **1995,** *28*, 329.

64. Puente, J. M., Alonso, F. J., Andres, L., Prado, M. In *Influence of an adequate surface conditioning on the final characteristics of GI for exposed panels use on automotive sector*, Galvatech '04 - Proc. 6th Int. Conf. on Zinc and Zinc Alloy Coated Steel Sheet, Chicago, USA; 2004, pp 457.

65. Du, D., Kim, S. -S., Moon, W. -S., Jin, S. -B., Kwon, W. -S., *Thermochim. Acta* **2003,** *407*, 17.

66. Komatsuzaki, S., Uematsu, T., *Lubr. Eng.* **1995,** *51*, 653.

67. Mansur, C. R. E., Gonzalez, G., Lucas, E. F., *Polym. Degrad. Stab.* **2003,** *80*, 579.

68. Santacesaria, E., Gelosa, D., Di Serio, M., Tesser, R., *J. Appl. Polym. Sci.* **1991,** *42*, 2053.

69. Sarpal, A. S., Christopher, J., Mukherjee, S., Patel, M. B., Kapur, G. S., *Lubr. Sci.* **2005,** *17*, 319.